Universidade do Minho
Escola de Engenharia

Karini Cristia Quaresma Nunes de Oliveira

Mechanical Characterisation of 3D Printed Sandwich Structures with Thermoplastic Core and Carbon Fibre Reinforcement

Mechanical Characterisation of 3D Printed Sandwich Structures with Thermoplastic Core and Carbon Fibre Reinforcement

Karini Cristia Quaresma Nunes de Oliveira

FRP++ Advanced structural analysis and design using composite materials

UMinho | 2025

FRP++
Advanced structural analysis and design using composite materials

Funded by the European Union

September 2026

The European Master in Advanced Structural Analysis and Design using Composite Materials is a join initiative of:

Universidade do Minho · Universitat de Girona · Università degli Studi di Napoli Federico II · INSA Institut National des Sciences Appliquées Toulouse · Université de Toulouse

Universidade do Minho
Escola de Engenharia

Karini Cristia Quaresma Nunes de Oliveira

Mechanical Characterisation of 3D Printed Sandwich Structures with Thermoplastic Core and Carbon Fibre Reinforcement

FRP++
Advanced structural analysis and design using composite materials

Master Dissertation
European Master Advanced Structural Analysis and Design using Composite Materials

Work developed under the supervision of
Doctor Luís Correia
Doctor Filipe Ribeiro

Funded by the European Union

September 2026

DIREITOS DE AUTOR E CONDIÇÕES DE UTILIZAÇÃO DO TRABALHO POR TERCEIROS

Este é um trabalho académico que pode ser utilizado por terceiros desde que respeitadas as regras e boas práticas internacionalmente aceites, no que concerne aos direitos de autor e direitos conexos.

Assim, o presente trabalho pode ser utilizado nos termos previstos na licença abaixo indicada.

Caso o utilizador necessite de permissão para poder fazer um uso do trabalho em condições não previstas no licenciamento indicado, deverá contactar o autor, através do RepositóriUM da Universidade do Minho.

Licença concedida aos utilizadores deste trabalho



Atribuição-NãoComercial-SemDerivações CC BY-NC-ND

https://creativecommons.org/licenses/by-nc-nd/4.0/

ACKNOWLEDGEMENTS

First and foremost, I would like to express my deepest gratitude to my parents. Without their love, support, encouragement, I would never have had the opportunity to pursue this Master's degree. There is so much in my life that I would not have been able to accomplish without them, and I am deeply grateful for everything they have done for me throughout my life. Thank you for believing in me, supporting my choices, and giving me the strength to keep going.

I would like to express my sincere gratitude to my supervisors, Luís and Filipe, for their guidance, knowledge, support, patience, and motivation throughout this work. I am deeply grateful for everything you have taught me and for the time and effort you dedicated to this thesis. Your guidance was essential to its completion, and this work would not have been possible without you.

I am very grateful to all my friends who were part of this journey. Thank you for your constant support, encouragement, and for believing in me. Thank you also for listening to all my complaints about everything that went wrong during this thesis, for making difficult days lighter, and for filling this journey with moments of laughter and happiness. Having you by my side made this journey much more enjoyable and meaningful.

A special thank you goes to Joanne and Sebastian. You were truly angels in my life during some of the most difficult moments of this journey. Thank you for helping me, encouraging me, and giving me strength whenever I needed it most. Your kindness meant more to me than I can put into words, and I will never forget it.

I would also like to thank my dear friend Alex. Our discussions, analyses, and jokes made the thesis much happier. Thank you for being there throughout this process, for helping me think through countless problems, and for making the long days of thesis work a little lighter. I could not have done it without you.

I would also like to thank all the professors of the FRP++ programme. Everything I have learned throughout this master’s degree is thanks to your knowledge, dedication, and efforts to teach us. I am deeply grateful for everything you have taught me and for the knowledge that I will carry with me into my professional career. A special thank you goes

to Professor Azoti, who taught me everything I know about Abaqus. I am especially grateful for your patience, availability, and for going beyond what could be expected from your role as a professor to help me whenever I needed it. Your support was invaluable throughout this work.

I would like to sincerely thank Edgar, from ISQ, for his help with the printing of the specimens used in this work. I am very grateful for his time, assistance, and willingness to help throughout the specimen manufacturing process.

I would also like to thank the team of the Laboratory of the University of Minho for their assistance during the experimental programme. I am particularly grateful for all the time, support, and knowledge shared with me throughout the testing process, which contributed significantly to the successful completion of this work.

I would like to acknowledge the European Union for the financial support provided through the Erasmus Mundus FRP++ European Master Course in Advanced Structural Analysis and Design using Composite Materials (Project No. 101048961).

I also gratefully acknowledge the financial support provided by FCT/MCTES through the R&D Unit Institute for Sustainability and Innovation in Structural Engineering (ISISE), under references UID/4029/2025, UID/PRR/04029/2025, and UID/PRR2/04029/2025, and through the Associate Laboratory Advanced Production and Intelligent Systems (ARISE), under reference LA/P/0112/2020.

Finally, I would like to acknowledge ISQ for the support provided during this work.

Finally, I would like to thank everyone who contributed to this journey. I am deeply grateful to all of you for your support and for being part of this chapter of my life.

STATEMENT OF INTEGRITY

I hereby declare having conducted this academic work with integrity. I confirm that I have not used plagiarism or any form of undue use of information or falsification of results along the process leading to its elaboration.

I further declare that I have fully acknowledged the Code of Ethics and Conduct of the University of Minho.

DECLARATION ON THE USE OF ARTIFICIAL INTELLIGENCE (AI) TOOLS

I hereby declare having acted this academic work with integrity and confirm that I have not resorted to any form of undue use of AI tools, nor to the falsification or omission of information, sources, data, results or processes in any of the stages leading to its elaboration.

I further declare that any use of AI tools was done in a transparent and responsible manner, being duly noted in the work, and that I critically verified the accuracy of the content produced with their support, assuming full responsibility for what I submit.

I further declare that I have fully acknowledged the Code of Ethics and Conduct of the University of Minho, as well as the applicable standards of academic integrity and data protection.

Caracterização Mecânica de Estruturas Sandwich Impressas em 3D com Núcleo Termoplástico e Reforço de Fibra de Carbono

RESUMO

As estruturas sandwich combinam camadas finas com um núcleo leve, alcançando uma elevada eficiência estrutural com baixo peso. O fabrico aditivo permite arquiteturas de núcleo complexas e fabrico integrado do núcleo e peles, eliminando a interface adesiva responsável por falhas prematuras em painéis convencionais. O reforço com fibra de carbono contínua pode melhorar o desempenho destes compósitos, mas a caracterização continua a ser um desafio pela dependência do processo de fabrico e pela escassez de normas de ensaio.

Esta dissertação investiga estruturas sandwich impressas em 3D num sistema Markforged Mark Two, com núcleo em Onyx® e peles em Onyx® reforçado com fibra de carbono contínua. Ambos foram caracterizados à tração e à flexão em duas orientações de impressão, seguindo-se ensaios de flexão em quatro pontos dos painéis. A orientação de impressão teve efeito limitado na resistência à tração do Onyx®, mas maior influência na rigidez e ductilidade; a 0°/90°, o reforço elevou a resistência e o módulo de 27,47 MPa e 0,73 GPa para 347,42 MPa e 23,41 GPa. Em flexão, o Onyx® atingiu 33,83 MPa e 1,54 GPa a 0°/90° e 42,30 MPa e 1,96 GPa a 45°/−45°, enquanto o material reforçado atingiu 115,61 MPa e 3,83 GPa, e 31,39 MPa e 1,20 GPa; o reforço melhorou o desempenho a 0°/90°, mas reduziu-o inesperadamente a 45°/−45°.

Os ensaios de flexão do sanduiche resultaram numa rigidez inicial média de 0,504 kN/mm e numa carga máxima de 1,81 kN aos 5,20 mm, com rotura por delaminação progressiva e localizada. Foi também desenvolvido um modelo de elementos finitos, com propriedades isotrópicas e núcleo simplificado, que reproduziu a força experimental com desvio inferior a 2%, mas subestimou a rigidez em cerca de 29%. No geral, este trabalho fornece uma caracterização experimental sólida e uma base numérica de referência para o desenvolvimento futuro deste tipo de estruturas.

PALAVRAS-CHAVE: Compósitos de Fabrico Aditivo; Markforged; Estruturas Sandwich; Onyx®; Reforço de Fibra de Carbono Contínua.

Mechanical Characterisation of 3D Printed Sandwich Structures with Thermoplastic Core and Carbon Fibre Reinforcement

ABSTRACT

Sandwich structures combine thin face sheets with a lightweight core, achieving high structural efficiency at low weight. Additive manufacturing (AM) enables complex core architectures and integrated core-face sheet fabrication, eliminating the adhesive interface that often causes premature failure in conventionally bonded panels. Continuous fibre reinforcement can further enhance AM composites, though characterisation remains challenging due to process-dependent properties and limited testing standards.

This thesis investigates 3D-printed sandwich structures manufactured on a Markforged Mark Two system, with an Onyx® core and continuous carbon fibre-reinforced Onyx® face sheets. Both materials were tensile and flexurally characterised under two printing bed orientations, followed by four-point bending tests of the sandwich panels. Printing orientation had limited effect on Onyx® tensile strength but a stronger influence on stiffness and ductility; continuous fibre reinforcement raised the 0°/90° tensile strength and modulus from 27.47 MPa and 0.73 GPa to 347.42 MPa and 23.41 GPa. In flexure, Onyx® reached 33.83 MPa and 1.54 GPa for 0°/90° and 42.30 MPa and 1.96 GPa for 45°/−45°, while the reinforced material reached 115.61 MPa and 3.83 GPa, and 31.39 MPa and 1.20 GPa; reinforcement improved flexural performance for 0°/90° but unexpectedly reduced it for 45°/−45°.

Four-point bending tests of the sandwich panels gave an average initial stiffness of 0.504 kN/mm and a maximum load of 1.81 kN at 5.20 mm, with failure governed by progressive, localised delamination rather than fracture. A finite element model, using isotropic properties and a simplified equivalent core, reproduced the experimental force within 2% but underestimated the stiffness by about 29%, mainly due to the core simplification. Overall, this work provides an experimentally grounded characterisation of this AM sandwich system and a numerical baseline for future design of this class of structures.

KEYWORDS: Additively Manufactured Composites; Markforged; Sandwich Structures; Onyx®; Continuous Carbon Fibre Reinforcement

TABLE OF CONTENTS

Acknowledgements iii
Caracterização Mecânica de Estruturas Sandwich Impressas em 3D com Núcleo Termoplástico e Reforço de Fibra de Carbono VI
Resumo VI
Abstract VII
Table of Contents VIII
List of Figures X
List of Tables XIV
List of Abbreviations and Symbols XVI
1. Introduction 1
1.1. Background and engineering relevance 1
1.2. Motivation 4
1.3. Objectives and expected results 4
1.4. Thesis Organization 5
2. Literature review 6
2.1. Conception, design and manufacture of Additively Manufactured Sandwich Structures 6
2.1.1. Materials used in additively manufactured composites 6
2.1.2. Markforged two process 8
2.1.3. Manufacturing variables affecting performance and limitations 9
2.2. Experimental characterisation strategies 14
2.3. Numerical modelling approaches 18
3. Experimental Programme and Methodology 20
3.1. Experimental Program 20
3.1.1. Materials 20
3.1.2. Specimen Design and Manufacturing 20
3.1.3. Experimental Programme Scope 25
3.1.4. Specimen Nomenclature 25

3.2. Experimental Equipment 26
3.3. Tensile Test of Printed Onyx® Specimens 27
3.4. Tensile Test of Printed Carbon Fibre Reinforced Onyx® Specimens 28
3.5. Flexural Test of Printed Onyx® Specimens 29
3.6. Flexural Test of Printed Continuous Carbon Fibre Reinforced Onyx® Specimens 30
3.7. Four-Point Bending Test of Sandwich Specimens 31
4. Experimental Results and Discussion 34
4.1. Tensile Behaviour of Printed Onyx® Specimens 34
4.2. Tensile Behaviour of Printed Carbon Fibre-Reinforced Onyx® Specimens 38
4.3. Flexural Behaviour of Printed Onyx® Specimens 41
4.4. Flexural Behaviour of Printed Carbon Fibre-Reinforced Onyx® Specimens 46
4.5. Four-Point Bending Test of Sandwich Specimens 52
5. Numerical Modelling 59
5.1. Finite Element Model 59
5.2. Numerical Results 62
5.3. Comparison of Numerical with Experimental Results 63
6. Conclusions and further developments 66
6.1. Main conclusions 66
6.2. Further developments 69
References 73
Annex I 75

LIST OF FIGURES

Figure 2.1: Representation of Markforged Mark Two printing system, illustrating the dual-nozzle configuration for thermoplastic deposition and continuous fibre placement [7]. 9
Figure 2.2: Printing parameters [7]. 10

Figure 3.1: Workflow adopted for the design, printing configuration, manufacturing, experimental characterisation and numerical modelling. 21
Figure 3.2: Markforged Mark Two printer used to manufacture the specimens: (a) build plate with completed specimens and the touchscreen interface; (b) detail of the print head, showing the plastic and continuous-fibre deposition nozzles. 21
Figure 3.2: Layer arrangement adopted for (a) fully solid Onyx® specimens, (b) continuous carbon fibre reinforced specimens and (c) sandwich specimens. 22
Figure 3.3: Representative Eiger printing configurations showing: (a) specimen orientation for a 0° build orientation; (b) specimen orientation for a 45° build orientation; (c1) Onyx® material configuration; (c2) Onyx® reinforced with continuous carbon fibre and sandwich material configuration; (d) layer configuration; (e) X-ray view and fibre configuration of the continuous carbon fibre reinforced material specimens; and (f) X-ray view and fibre configuration of the sandwich specimens. 24
Figure 3.4: Experimental equipment used throughout the experimental programme: (a) MTS Exceed E45.105 universal testing machine; (b) MTS Advantage (AVX) video extensometer system. 27
Figure 3.5: Geometry and dimensions of the Onyx® tensile specimen. 27
Figure 3.6: Experimental setup used for the tensile tests. 28
Figure 3.7: Tensile test specimens: (a) specimen without tabs, showing premature failure in the gripping region; (b) specimen with bonded tabs adopted for the final testing procedure. 29
Figure 3.8: Experimental setup used for the three-point bending tests of Onyx® specimens. 30
Figure 3.9: Experimental setup used for the three-point bending tests of Carbon fibre-reinforced Onyx® specimens. 31

Figure 3.10: Sandwich specimen prepared for the four-point bending test, showing the speckle pattern applied to the lateral surface for optical deformation measurement. 32
Figure 3.11: Four-point bending test setup for the sandwich specimens: (a) schematic representation of the loading configuration according to DIN 53 293; (b) experimental setup used in the present study. 33

Figure 4.1: Onyx® tensile specimens manufactured for testing: (a) 0°/90° printing bed orientation; (b) 45°/−45° printing bed orientation. 34
Figure 4.2: Onyx® tensile specimens after testing: (a) 0°/90° printing bed orientation; (b) 45°/−45° printing bed orientation. 35
Figure 4.3: Close-up views of the fracture regions of the Onyx® tensile specimens: (a) 0°/90° printing bed orientation; (b) 45°/−45° printing bed orientation. 35
Figure 4.4: Engineering stress–strain curves obtained from the tensile tests of printed Onyx® specimens: (a) 0°/90° printing bed orientation; (b) 45°/−45° printing bed orientation. 36
Figure 4.5: Carbon fibre-reinforced Onyx® tensile specimens before testing: (a) specimens 1–5; (b) specimens 6–8. 38
Figure 4.6: Close-up views of the carbon fibre-reinforced Onyx® tensile specimens before testing, highlighting the observed manufacturing imperfections: (a) slight lateral curvature; (b) bubbles in the outer layer and curvature of the continuous carbon fibre. 38
Figure 4.7: Carbon fibre-reinforced Onyx® tensile specimens after testing: (a) specimens 3–5; (b) specimens 6–8. 39
Figure 4.8: Close-up view of the fracture region of carbon fibre-reinforced Onyx® tensile. .. 39
Figure 4.9: Engineering stress–strain curves obtained from the tensile tests of carbon fibre-reinforced Onyx® specimens. 40
Figure 4.10: Onyx® flexural specimens before testing: (a) 0°/90° printing bed orientation; (b) 45°/−45° printing bed orientation. 42
Figure 4.11: Onyx® flexural specimens after testing: (a) front view of specimens with 0°/90° printing bed orientation; (b) lateral view of the same specimens; (c) front view of specimens with 45°/−45° printing bed orientation; (d) lateral view of the same specimens. 43
Figure 4.12: Onyx® flexural specimen during testing, showing displacement from the supports at large deformation. 43

Figure 4.13: Engineering stress–strain curves obtained from the flexural tests of Onyx® specimens: (a) 0°/90° printing bed orientation; (b) 45°/−45° printing bed orientation. 44
Figure 4.14: Determination of the maximum flexural stress and corresponding strain from a representative Onyx® specimen, based on the stable portion of the stress–strain curve. 45
Figure 4.15: Carbon fibre-reinforced Onyx® flexural specimens before testing: (a) 0°/90° printing bed orientation; (b) 45°/−45° printing bed orientation. 47
Figure 4.16: Carbon fibre-reinforced Onyx® flexural specimen during testing, showing displacement from the supports at large deformation. 47
Figure 4.17: Carbon fibre-reinforced Onyx® flexural specimens after testing: (a) front view of specimens with 0°/90° printing bed orientation; (b) lateral view of the same specimens; (c) front view of specimens with 45°/−45° printing bed orientation; (d) lateral view of the same specimens. 48
Figure 4.18: Engineering stress–strain curves obtained from the flexural tests of carbon fibre-reinforced Onyx® specimens: (a) 0°/90° printing bed orientation; (b) 45°/−45° printing bed orientation. 49
Figure 4.19: Example of the determination of the maximum flexural stress and corresponding strain from the stable portion of the stress–strain curve. 50
Figure 4.20: Surface imperfections observed on the manufactured sandwich specimens before testing. 52
Figure 4.21: Sandwich specimens before the four-point bending tests: (a) top view; (b) lateral view. 52
Figure 4.22: Sandwich specimen during the four-point bending test. 53
Figure 4.23: Sandwich specimens after the four-point bending tests: (a) top view; (b) lateral view. 53
Figure 4.24: Load–displacement curves obtained from the four-point bending tests of the sandwich specimens, corrected for the initial seating region. 54
Figure 4.25: Close-up view of the post-test damage observed in each specimen: (a) S-F-0-0.90-1; (b) S-F-0-0.90-2; (c) S-F-0-0.90-3. 54
Figure 4.26: Load–strain curves obtained from the bottom mid-span strain gauge (SG1) during the four-point bending tests of the sandwich specimens (S-F-0-0.90) 56

Figure 5.1: Finite element model assembly: sandwich specimen (face sheets, Onyx® layers and core) and the four rollers used to reproduce the four-point bending fixture. 59
Figure 5.2: Mesh of the numerical model. 61
Figure 5.3: Force-displacement curve obtained from the numerical model, combining the reaction forces at the two loading rollers. 62
Figure 5.4: Deformed shape of the model (U2 displacement contour) at the final increment, corresponding to a prescribed displacement of 6 mm. 63
Figure 5.5: Comparison between the numerical force-displacement curve and the experimental curves of the three S-F-0-0.90 specimens. 65

LIST OF TABLES

Table 2.1: Reported mechanical properties of Onyx®, CCF-reinforced composite and carbon fibre. 8

Table 2.2: Influence of printing parameters on the tensile behaviour of Onyx® specimens, based on experimental results reported by Burnett *et al.* [7]. 13

Table 2.3: Main test methods and corresponding standards considered in the experimental programme reported by Liew *et al.* [15] for the material and structural characterisation of additively manufactured composite sandwich structures. 16

Table 2.4: Summary of material properties and structural stiffness of a Markforged-based CFRP/nylon sandwich system reported by Liew [15] under four-point bending tests. 17

Table 3.1: Nominal cross-section of the sandwich specimens, as defined in the Eiger slicing software. 22

Table 3.2: Main printing parameters adopted for the manufactured specimens. 23

Table 3.3: Specimen identification system adopted in this work. 25

Table 3.4: Experimental equipment used for the mechanical characterisation of the printed specimens. 26

Table 3.5: Summary of the Onyx® tensile specimens tested. 27

Table 3.6: Summary of the continuous carbon fibre reinforced Onyx® tensile specimens tested 28

Table 3.7: Summary of the Onyx® flexural tested specimens. 30

Table 3.8: Summary of the continuous carbon fibre reinforced Onyx® flexural test specimens. 31

Table 3.9: Summary of the sandwich specimens tested. 31

Table 4.1: Mechanical properties obtained from the tensile tests of printed Onyx® specimens. 37

Table 4.2: Tensile properties obtained for the carbon fibre-reinforced Onyx® specimens according to manufacturing condition. 41

Table 4.3: Flexural properties obtained for the Onyx® specimens according to printing bed orientation. 45
Table 4.4: Flexural properties obtained for the carbon fibre-reinforced Onyx® specimens according to printing bed orientation. 51
Table 4.5: Summary of the four-point bending test results obtained for the sandwich specimens from the crosshead displacement. 55
Table 4.6: Bending moment, strain and bending rigidity obtained for the sandwich specimens from the strain gauge (SG1) and from the crosshead displacement. 57

Figure 5.1: Finite element model assembly: sandwich specimen (face sheets, Onyx® layers and core) and the four rollers used to reproduce the four-point bending fixture. 59
Figure 5.2: Mesh of the numerical model. 61
Figure 5.3: Force-displacement curve obtained from the numerical model, combining the reaction forces at the two loading rollers. 62
Figure 5.4: Deformed shape of the model (U2 displacement contour) at the final increment, corresponding to a prescribed displacement of 6 mm. 63
Figure 5.5: Comparison between the numerical force-displacement curve and the experimental curves of the three S-F-0-0.90 specimens. 65

LIST OF ABBREVIATIONS AND SYMBOLS

Abbreviations

ABS	Acrylonitrile Butadiene Styrene
AM	Additive Manufacturing
ASTM	American Society for Testing and Materials
ALLSD	Energy dissipated by automatic stabilisation
ALLIE	Internal strain energy of the model
BS	British Standard
CAD	Computer-Aided Design
CCF	Continuous Carbon Fibre
CFF	Continuous Filament Fabrication
CFRP	Carbon Fibre-Reinforced Polymer
CT	Computed Tomography
DIC	Digital Image Correlation
DIN	Deutsches Institut für Normung
EN	European Norm
FE	Finite Element
FEA	Finite Element Analysis
FFF	Fused Filament Fabrication
ISO	International Organization for Standardization
ISQ	Instituto de Soldadura e Qualidade
ME	Material Extrusion
PA	Polyamide
PA6	Polyamide 6
PC	Polycarbonate
PETG	Polyethylene Terephthalate Glycol
PLA	Polylactic Acid
SG	Strain Gauge

Symbols

σ	Stress
ε	Strain
E	Modulus (tensile/flexural, as specified in context)
P	Load
δ	Displacement
M	Bending moment
k	Stiffness
EISG	Bending rigidity, from strain gauge
EIcross	Bending rigidity, from crosshead displacement
d	Distance between face-sheet centroids
t	Face-sheet thickness
b	Panel width
a	Support-to-load distance
L	Support span
h	Total sandwich panel thickness

THIS PAGE WAS INTENTIONALLY LEFT BLANK

1. INTRODUCTION

1.1. Background and engineering relevance

Sandwich structures are widely used in various engineering applications due to their favourable combination of low weight, high stiffness, and structural efficiency [1]. In general, a sandwich structure consists of two thin face sheets separated by a lightweight core, resulting in an efficient structural configuration. The structural efficiency of sandwich panels is achieved through the separation of the face sheets by the core, which increases the section's moment of inertia. In this configuration, the face sheets mainly resist tensile and compressive stresses, whereas the core carries shear loads and stabilises the faces against local buckling [2].

However, the manufacture of sandwich structures still presents some limitations, particularly regarding the quality and reliability of the bond between the core and the face sheets. In conventional sandwich panels, the face sheets and core are typically manufactured separately and subsequently joined by adhesive bonding. As a result, the bonded interface may become a critical region affecting the structural performance of the component, since premature failure often initiates by delamination at the adhesive layer [3], [4].

To overcome these manufacturing limitations, additive manufacturing (AM) has emerged as a promising alternative fabrication route for sandwich structures. Unlike conventional manufacturing methods, AM enables the fabrication of integrated sandwich components, reducing assembly operations and potentially eliminating the adhesive interface between the core and the face sheets. This integrated manufacturing approach has the potential to improve the structural integrity of sandwich components by avoiding one of the principal sources of failure associated with conventional bonded assemblies [5].

AM is a manufacturing process in which components are built layer by layer directly from digital 3D models. In recent years, its adoption has grown significantly as an alternative to traditional manufacturing techniques, driven primarily by its advantages in rapid prototyping and automated production. The growing interest in 3D printing is largely related to its ability to automate fabrication, produce multiple parts efficiently, offer flexibility in material usage and manufacture components that closely resemble final products [6]. More broadly, AM has been transforming modern manufacturing by enabling the fabrication of complex geometries

with reduced material waste [7]. In addition, the layer-by-layer fabrication process provides unprecedented design freedom, making it possible to manufacture intricate internal architectures and customized structures that would be difficult or impossible to produce using conventional manufacturing methods [8]. These capabilities are particularly attractive for sandwich structures, as they enable complex core geometries to be manufactured while also allowing the core and face sheets to be fabricated as a single integrated component.

The benefits of this integrated manufacturing approach have been demonstrated by Nishi *et al.* [5], who investigated the integral fabrication of continuous carbon-fibre-reinforced polymer (CFRP) sandwich structures using additive manufacturing. The authors identified the adhesive layer as a major limitation of conventionally manufactured sandwich panels, where delamination often leads to premature failure before the full mechanical capacity of the structure is reached. To overcome this limitation, they manufactured the sandwich panels as a single integrated component using a Markforged Mark Two printer, thereby eliminating the adhesive interface. Experimental three-point bending tests showed that conventionally manufactured specimens failed by delamination at the adhesive layer, whereas integrally manufactured specimens failed within the core and face sheets. Consequently, the integrally manufactured specimens exhibited superior mechanical performance because premature adhesive-layer failure was avoided.

In addition to these manufacturing advantages, AM is particularly compatible with fibre-reinforced polymer composites, which are widely used in high-performance engineering applications due to their high strength-to-weight ratio, corrosion resistance, and favourable mechanical properties [9]. In AM composites, reinforcement can be introduced either in the form of short fibres already incorporated into the filament or as continuous fibres embedded during the printing process [7], [10]. Short fibre-reinforced systems can improve the mechanical behaviour when compared to unreinforced polymers, but their structural performance remains limited for more demanding applications [6], [11]. For this reason, continuous fibre-reinforced systems have received increasing attention due to their greater potential to enhance the stiffness and strength of printed components [12].

In particular, the development of fibre-reinforced composites through AM has opened new possibilities for the design of high-performance components [10], [13]. These technologies allow not only the fabrication of complex and customised geometries, but also the control of fibre orientation and even the placement of curvilinear fibres, which expands the design

freedom of composite structures [13]. This is especially relevant because continuous fibre-reinforced polymer composites are already widely used in aerospace, automotive, and marine applications, while fibre orientation and fibre path design play a major role in determining the mechanical performance of the final part [14]. Therefore, AM shows strong potential for the fabrication of composite structures with tailored mechanical behaviour.

Despite this potential, the design and manufacture of AM composite structures remain complex and still require considerable expertise. Current methodologies often focus on optimising isolated stages of the process rather than considering the full design-to-manufacturing route in an integrated way, which highlights the need for more comprehensive approaches [10]. In addition, the characterisation of AM composites remains challenging because their mechanical behaviour depends strongly on processing conditions and material uncertainties [6].

Unlike conventional composites, their properties are affected not only by the fibre and matrix constituents, but also by the printing technology, processing parameters, environmental conditions, and possible post-processing operations [6]. Parameters such as raster angle, layer configuration, and manufacturing defects introduce additional variability, making the mechanical response more difficult to predict [6], [15]. Although the growing range of applications is promising, there is still significant variation in the performance of 3D-printed composites, and a more systematic understanding of the influence of slicing and processing parameters is still needed [7].

As highlighted by Liew *et al.* [15] , these challenges are further aggravated by the dependence on manufacturer-provided material data, which may be incomplete or subject to updates, as well as by practical difficulties during specimen fabrication and testing, such as moisture-related issues and printing defects. As a result, obtaining accurate and reproducible stiffness properties is not straightforward, and even carefully planned experimental programmes may lead to incomplete or inconclusive results. This reinforces the need for further studies focused on the mechanical characterisation of AM composite structures.

In view of these challenges, this thesis focuses on the mechanical characterisation and structural behaviour of AM solutions, namely on sandwich structures composed of a cellular Onyx® core and continuous carbon fibre-reinforced face sheets, manufactured using the Markforged Mark Two. In this context, Onyx® is used as the matrix material, while continuous carbon fibre is used as reinforcement. To investigate this behaviour, the work combines

experimental testing with numerical modelling, aiming to improve the understanding of structural performance of these printed configurations. By addressing these aspects, the thesis intends to contribute to the current understanding of 3D-printed composite sandwich structures and to support their future development for lightweight engineering applications.

1.2. Motivation

Despite the potential outlined in the previous section, the mechanical behaviour of Onyx®continuous carbon fibre sandwich structures manufactured on the Markforged Mark Two system remains largely uncharacterised, particularly at the level of the assembled, printed panel. The properties of the constituent Onyx® and continuous carbon fibre-reinforced materials do not, on their own, allow the structural response of the printed sandwich to be predicted, since this response also depends on manufacturing-related factors specific to the assembled structure that cannot be inferred from material-level data alone. Because no standard currently addresses AM sandwich structures specifically, published data on this exact configuration is limited to a handful of isolated studies rather than an established characterisation framework, leaving designers without a reliable basis for predicting structural performance before building and testing a given design. This gap is the motivation for the present work, which is centred on the experimental characterisation of the printed sandwich structure itself under four-point bending, together with the constituent materials from which it is made, and a preliminary numerical model to help interpret the results and provide a starting point for future design decisions

1.3. Objectives and expected results

The main objective of this thesis is to investigate the mechanical and structural behaviour of AM sandwich structures composed of an Onyx® core and continuous carbon fibre-reinforced face sheets, manufactured using the Markforged Mark Two. More specifically, the work aims at (i) experimentally determining the stiffness-related properties of Onyx® and continuous carbon fibre-reinforced Onyx® through tensile and flexural testing; (ii) evaluating the global response of the sandwich panels under flexural loading in order to obtain effective structural

properties; and (iii) using finite element simulations to interpret the experimental results and support the understanding of the structural response.

The expected outcome is an improved understanding of how the properties of the printed materials contribute to the behaviour of the full sandwich structure. In addition, the work is expected to provide a set of experimentally supported material and structural data, together with a preliminary numerical model that can serve as a starting point for the future design of 3D-printed composite sandwich systems.

1.4. Thesis Organization

Chapter 1 introduces the research context, motivation, objectives and scope of the study. Chapter 2 presents the fundamentals of additive manufacturing and the processes, materials and printing parameters relevant to the production of composite structures. It then discusses the factors governing the quality and mechanical behaviour of printed specimens, approaches for their experimental characterisation and numerical modelling, and the development of additively manufactured sandwich structures. Previous studies are reviewed to assess the current state of knowledge, their main findings and the challenges and limitations that remain. Chapter 3 describes the experimental approach adopted in this work, including specimen design and manufacturing, the selected testing standards and experimental equipment, and the procedures used to characterise the printed materials and evaluate the sandwich structures. Chapter 4 presents and discusses the experimental results, assessing the influence of the investigated manufacturing configurations and reinforcement and establishing comparisons between the tested specimens and, where appropriate, manufacturer-reported values and previous studies. Chapter 5 builds on the experimental results through finite element modelling of the sandwich structure under four-point bending and evaluates the numerical response in relation to the experimental behaviour. Finally, Chapter 6 summarises the main conclusions and identifies opportunities for further development.

2. LITERATURE REVIEW

2.1. Conception, design and manufacture of Additively Manufactured Sandwich Structures

2.1.1. Materials used in additively manufactured composites

AM can process a wide range of materials, including polymers, metals, ceramics, and composites. However, material-extrusion technologies remain predominantly based on thermoplastic polymers, such as acrylonitrile butadiene styrene (ABS), polylactic acid (PLA), polycarbonate (PC), polyamide (PA), nylon, and polyethylene terephthalate glycol (PETG), owing to their processability and compatibility with extrusion-based printing systems [16].

Among the materials employed in AM composites, thermoplastic matrices have become increasingly relevant. Although thermoplastics generally exhibit lower strength than thermosets, they offer important advantages such as shorter fabrication times, higher strain-to-failure, and the possibility of reprocessing and recycling, making them particularly suitable for additive manufacturing applications [11].

Among the thermoplastic materials employed in additively manufactured composites, Onyx® has gained particular attention. Kumar *et al*. [9] describe Onyx® as a high-performance material developed by Markforged, consisting of a polyamide 6 (PA6), or nylon, matrix reinforced with chopped carbon fibres. The incorporation of chopped carbon fibres enhances the mechanical performance of the material, increasing the tensile modulus by approximately 21.5% and the ultimate tensile strength by 23.5% compared with unreinforced nylon, although this improvement may occur at the expense of ductility, resulting in a significant reduction in strain at break [7]. In addition to its improved mechanical properties, Onyx® offers enhanced dimensional stability, wear resistance, and thermal tolerance, making it suitable for engineering applications requiring lightweight and durable components [9]. Consequently, Onyx® has seen increasing adoption in aerospace and automotive applications due to its favourable strength-to-weight ratio, stiffness, and manufacturability. Reported

applications include non-structural aircraft components, UAV frames, satellite brackets, lightweight tooling, and custom fixtures [7].

While chopped-carbon-fibre-reinforced thermoplastics already provide an important improvement over unreinforced polymers, higher structural performance is generally achieved when continuous fibres are used as reinforcement. Continuous Filament Fabrication (CFF) presents substantially higher strength and stiffness, making them more suitable for demanding structural applications than short-fibre-reinforced systems. The tensile strength and tensile modulus of Continuous Carbon Fibre (CCF) composite materials have been reported to be 21.82 and 21.15 times higher, respectively, than those of short-fibre-reinforced composite materials [16].

In Markforged-type systems, Onyx® acts as the matrix material while continuous carbon fibre is introduced as reinforcement, resulting in a hybrid composite system capable of achieving substantially higher mechanical properties than the matrix material alone. Zehni *et al.* [6] report manufacturer values of 2.4 GPa tensile modulus and 40 MPa tensile yield stress for the Onyx® matrix filament, while the continuous carbon fibre filament is reported with a tensile modulus of 60 GPa and a tensile strength of 800 MPa. **Table 2.1** compares the manufacturer-supplied mechanical properties of Onyx® and carbon fibre [17] and the continuous-carbon-fibre-reinforced composite reported by Dong [18], highlighting the substantial increase in stiffness and strength achieved through continuous fibre reinforcement.

These values illustrate the potential increase in stiffness and strength associated with the incorporation of continuous carbon fibre compared with the Onyx® matrix. However, the properties of a CCF-reinforced printed composite are strongly dependent on the specific fibre content, orientation, number and arrangement of fibre layers, and specimen configuration. Therefore, the values reported by Dong [18] aren´t used as direct comparison values for the CCF-reinforced specimens tested in the present study.

Table 2.1: Reported mechanical properties of Onyx®, CCF-reinforced composite and carbon fibre.

Property	**Onyx®****	**CCF-reinforced composite***	**Carbon fibre****
Tensile modulus (GPa)	2.4	60	60
Tensile strength (MPa)	37	800	800
Tensile stress at yield (MPa)	40	–	–
Tensile strain at break (%)	25	–	1.5
Flexural strength (MPa)	71	–	540
Flexural modulus (GPa)	3.0	–	51
Flexural strain at break (%)	–	–	1.2
Compressive modulus (GPa)	–	54	62
Compressive strength (MPa)	–	320	420
Notes: * Values reported by Dong [18] based on manufacturer-supplied data. ** Values reported by Markforged [19].			

2.1.2. Markforged two process

Material extrusion (ME) is an additive manufacturing process in which a material is heated and deposited layer by layer to build a 3D structure. In this process, the printed structure is formed by the sequential deposition of individual filaments, commonly referred to as beads, which are arranged side by side and may contain voids between adjacent paths [10], [12].

Fused Filament Fabrication (FFF) is a branch of ME, consisting of the deposition of an extruded filament onto the printing bed or onto previously deposited layers [10]. This technique has gained widespread adoption due to its low cost and ease of use [7]. However, the mechanical performance of FFF-based parts remains a key challenge, particularly for load-bearing applications, which has led to the development of fibre-reinforced composite materials to enhance their mechanical properties [7].

In addition to conventional polymer printing, FFF-based systems can be used to manufacture fibre-reinforced composites. Short fibre-reinforced composites can be fabricated using composite filaments such as Onyx®, in which the reinforcement is already incorporated into the material. In addition, FFF printers have also been shown to produce continuous fibre-reinforced composites through specialised configurations [20]

Continuous Filament Fabrication (CFF) is a technique in which continuous fibres are embedded within the thermoplastic matrix during the printing process. This approach improves mechanical properties and enables control of fibre orientation within the printed structure [6]. The method has attracted considerable attention, particularly in studies investigating the tensile and flexural behaviour of continuous fibre-reinforced printed composites [6]. A

commercial system implementing this approach is the Markforged Mark Two. Kumar *et al.* [9] describe this printer as a professional-grade system for the fabrication of high-strength composite parts, integrating FFF in the first nozzle for deposition of the polymer matrix and CFF, in the second nozzle for embedding continuous fibres. The dual-nozzle configuration of this system is illustrated in **Figure 2.1.**

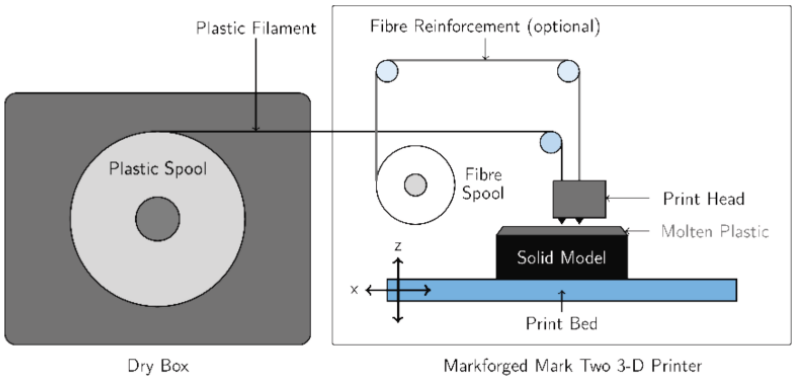


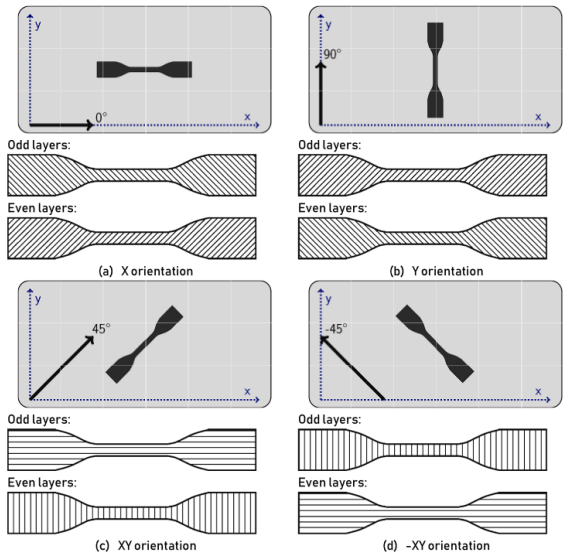
Figure 2.1: Representation of Markforged Mark Two printing system, illustrating the dual-nozzle configuration for thermoplastic deposition and continuous fibre placement [7].

The Markforged Mark Two operates using the proprietary cloud-based slicing software Eiger, which is used to prepare the printing process. In general, the workflow involves exporting a CAD model as an STL file and defining parameters such as material type, layer height, infill structure, and part orientation. The software can also provide estimates of print time, material consumption, fibre volume, and cost [7], [15]. During printing, the thermoplastic filament is heated and extruded through the nozzle onto the print bed or previously deposited layers, and the part is built layer by layer [7]. In this process, the orientation of the deposited filaments is associated with the alignment of fibres within the structure, which contributes to anisotropic mechanical behaviour [13].

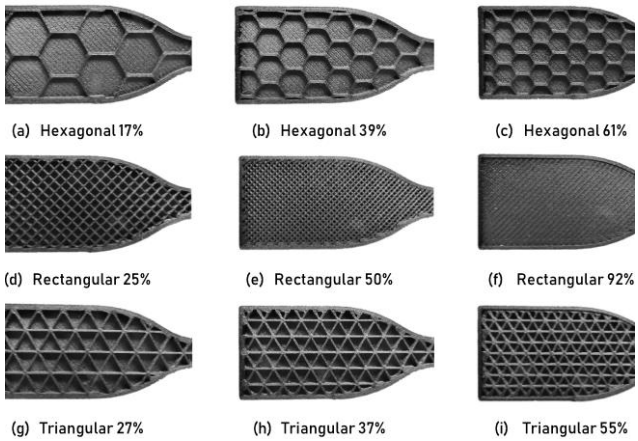
2.1.3. Manufacturing variables affecting performance and limitations

The mechanical performance of fibre-reinforced 3D-printed composites is highly dependent on slicing and processing variables. Among the most relevant are raster angle, print orientation, infill pattern, infill density, layer thickness, number of walls, and the number of

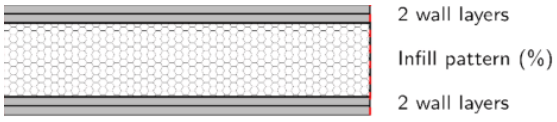
roof and floor layers [7]. These variables define the material deposition strategy and strongly influence the internal architecture of the printed part, as illustrated in **Figure 2.2**.



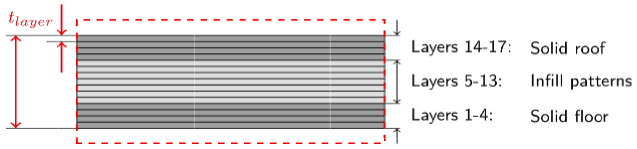
(a) Raster angle and print orientation configurations.



(b) Infill patterns and density variations.



(c) Representation of wall layers and infill pattern.



(d) Representation of roof and floor layers, infill pattern and thickness of the layer.

Figure 2.2: Printing parameters [7].

Among these, print orientation and raster angle deserve particular attention because they determine the alignment of the deposited filaments with respect to the loading direction. Print orientation refers to the orientation of the part on the printing bed during manufacture and can be adjusted according to the desired build configuration. In contrast, the raster angle describes the orientation of the deposited filament with respect to a reference direction of the printed part [7]. Liew [15] identified these variables, together with infill type, infill density and the number of walls, as the factors that most significantly affect the stiffness, strength and ductility of printed components.

Although print orientation and raster angle are often treated as independent variables in conventional FFF systems, this relationship differs in Markforged printers. According to Kumar and Kumar [21], the Eiger slicing software generates the polymer matrix using predefined alternating raster orientations of +45° and −45°, while the continuous fibre lay-up can be defined independently by the user. Consequently, unlike the print orientation, which can be

freely adjusted by rotating the part on the printing bed, the matrix raster is constrained by the slicing strategy.

To investigate the influence of filament alignment without altering the predefined deposition strategy, several authors have therefore used the print orientation as an indirect means of modifying the effective raster orientation relative to the loading direction. For example, Sangaletti *et al.* [22] obtained specimens with an effective 0°/90° raster configuration by rotating the part by 45° on the printing bed while maintaining the same matrix deposition strategy. Therefore, in Markforged composite systems, the alignment of the polymer matrix with respect to the loading direction can be modified through the build orientation of the part, whereas the continuous fibre reinforcement offers considerably greater design flexibility, allowing fibres to be deposited at multiple angles, including isotropic [0°/45°/90°/135°] and user-defined lay-ups.

At the mesostructural level, FFF components are formed by the sequential deposition of individual filaments, commonly referred to as beads, which are placed side by side to build each printed layer. However, voids may remain between adjacent beads, affecting the continuity of the material. Polyzos *et al.* [12] showed that such voids reduce stress transfer between neighbouring beads and contribute to progressive damage mechanisms. Experimental observations by Kubota et al. [20] likewise confirmed the presence of voids and weak fusion between adjacent print paths. In some configurations, particularly for ±45° raster orientations, larger gaps between neighbouring paths were observed, contributing to lower tensile strength [12], [20].

Previous studies, as discussed by Burnett *et al.* [7], indicate that unidirectional prints with a raster angle of 0° tend to achieve higher tensile strength and stiffness, while performance generally decreases as the raster angle approaches 90°. Nevertheless, the effect of raster angle is strongly influenced by interactions with other printing variables, meaning that its influence cannot be evaluated independently. As a result, the trends reported in the literature and in specific experimental studies should be understood as configuration-dependent rather than as universal rules. For this reason, no clear consensus exists regarding whether configurations such as 0°/90° or ±45° provide universally superior mechanical properties.

A similar dependence on the overall manufacturing configuration is also observed for other process variables. Layer thickness, defined as the height of each deposited layer, is another

factor that affects mechanical performance. Its influence is not uniform across studies, precisely because it interacts with other printing conditions and with the material system considered [7]. For the Markforged Mark Two, the Eiger software provides three selectable layer thicknesses for Onyx® deposition: 0.100 mm, 0.125 mm and 0.200 mm.

Besides raster angle and layer thickness, the mechanical response of FFF components is also influenced by the infill strategy and the configuration of the outer solid layers. In the Eiger slicing software, the internal architecture is defined by the selected infill pattern and infill density. Different infill geometries, including hexagonal, rectangular, triangular and solid configurations, influence stress distribution and failure mechanisms, thereby affecting structural integrity. In general, increasing infill density improves tensile strength and stiffness, although it also increases printing time and material consumption. However, the magnitude of this improvement depends on both the selected infill geometry and the overall printing configuration [7]. Similarly, Kumar *et al.* [9] identified infill pattern, fibre orientation and the number of roof layers as key variables governing the mechanical behaviour of printed composites.

In addition to the internal infill, the top and bottom surfaces of the component are formed by solid layers, referred to as roof and floor layers, whose number is selected in the Eiger slicing software[7]. Kumar *et al.* [9], in a study on 3D-printed Onyx®–glass fibre composites, found that the number of roof layers was the most influential variable among those investigated, producing a greater effect on tensile strength and hardness than infill pattern or infill orientation. In that study, the highest tensile strength and hardness were achieved using six roof layers in combination with a honeycomb infill and a 45° infill orientation.

The main trends observed in the experimental results reported by Burnett *et al.* [7] are summarised in Table 2.2. These trends should be interpreted in the context of the specific Onyx® configurations investigated, since the mechanical response depends on the interaction between multiple printing parameters and no single parameter can be considered universally optimal.

Table 2.2: Influence of printing parameters on the tensile behaviour of Onyx® specimens, based on experimental results reported by Burnett *et al.* [7].

Category	Configuration	Effect on Mechanical Behaviour
Print bed orientation	X / Y*	Produced ±45° raster layers relative to loading direction and showed superior tensile performance.
	XY / −XY*	Produced 0°/90° raster relative to loading direction, with higher tensile strength and stiffness and showed reduced tensile strain compared with X and Y orientations.
Layer thickness	0.125 mm	Highest tensile strength and modulus observed for Onyx®.
	0.100 mm	Lower tensile performance.
	0.200 mm	Lower tensile performance.
Infill pattern / density	Hexagonal	Stronger benefit from increasing density, especially at high density.
	Rectangular	Little change at low-to-mid density, but strong improvement at high density; 92% was close to solid.
	Triangular	Least sensitive to density increase; low densities already gave similar performance.

Notes:
*The printing orientations X, Y, XY and −XY are defined in **Figure 2.2**

Beyond the user-defined printing variables discussed previously, the manufacture of additively manufactured composite structures is also subject to several process-related constraints that must be considered during the design stage. In continuous-fibre printing systems, these limitations arise not only from the physical dimensions of the fibres, but also from machine tolerances, device limitations and predefined software restrictions, all of which reduce the range of feasible configurations [10].

In commercial systems such as the Markforged Mark Two, several processing conditions, including nozzle temperature, extrusion rate and printing speed, are predefined by the proprietary Eiger software and cannot be adjusted by the user [15]. Kubota *et al*. [20] similarly note that Markforged does not disclose the complete processing conditions, preventing direct access to several manufacturing variables. Although this simplifies the printing workflow, it also limits process optimisation and experimental flexibility.

In addition to these software limitations, the reinforcement strategy is also subject to manufacturing constraints. Liew [15] reports that, in the Markforged system, continuous fibre layers are always encapsulated by thermoplastic material. This predefined configuration improves process stability and printing consistency, but reduces the achievable fibre volume fraction and, consequently, limits the maximum mechanical performance of the printed component. Furthermore, the deposition of continuous fibres must follow feasible printing paths, which further restricts the range of geometries and reinforcement layouts that can be manufactured [15], [20].

Despite these manufacturing constraints, the orientation of the continuous fibre reinforcement remains one of the most influential design variables in additively manufactured composite structures. In structural design, fibre orientation plays a fundamental role in determining the mechanical strength of composite components, and improved performance can be achieved by optimising the fibre path within the structural domain [14]. In FFF composites, this effect is particularly important because the deposited fibres are aligned with the printing path, resulting in direction-dependent mechanical behaviour [20]. Consequently, numerical modelling approaches commonly represent this behaviour by assigning material orientations that follow the printing paths [13]. Accurate experimental characterisation of this anisotropic behaviour is therefore essential for understanding the mechanical response of additively manufactured composites and for developing reliable numerical models.

2.2. Experimental characterisation strategies

The characterisation of additively manufactured composite sandwich structures generally requires a combination of experimental testing, analytical methods, and numerical modelling. Experimental procedures are essential for determining the mechanical properties, while theoretical and numerical approaches help to interpret the results. In Liew [15], tensile tests were combined with micromechanical calculations and Classical Laminate Theory (CLT) to estimate the effective properties of printed CFRP layers, while finite element (FE) modelling was used to support the analysis of sandwich structures.

When interpreting these results, it is important to recognise that the filaments used in these systems do not represent pure constituent materials. As discussed by Kaushik *et al.* [11], the matrix filament already contains short carbon fibres, while the reinforcement filaments also include a polymer coating required for processing and bonding during deposition. Consequently, the specimens used for mechanical characterisation are produced from composite filaments whose internal composition must be considered when relating the measured properties to the behaviour of their individual constituents.

The mechanical response of printed composites is also strongly influenced by fibre distribution and orientation. In continuous fibre-reinforced systems, the reinforcement direction has a major influence on stiffness and strength, leading to pronounced anisotropy. Kaushik *et al.*

[11] demonstrated a strong influence of fibre orientation on flexural behaviour. A similar directional dependence is also observed in short-fibre systems. Kubota *et al.* [20] showed that, although the thermoplastic matrix itself is isotropic, printed parts become anisotropic because the fibres tend to align with the print path. In their Mark Two specimens, the 0° configuration exhibited substantially higher tensile strength and modulus than the other tested orientations.

The heterogeneous nature of these materials, together with the different mechanisms governing their behaviour at the constituent, bead, and structural levels, makes the prediction of their mechanical performance particularly challenging. To better capture these interactions, recent studies have adopted multi-scale approaches that relate behaviour across different length scales. For example, Polyzos *et al.* [12] linked fibre–matrix interactions at the bead scale to the global structural response of additively manufactured composite structures.

Given these sources of variability, reliable material characterisation requires carefully designed experimental procedures. However, Liew *et al.* [15] notes that no specific test standard is currently available for the material characterisation of additively manufactured CFRP plates or sandwich panels. Consequently, conventional standards originally developed for polymers, CFRP laminates, and sandwich structures were adopted as guidelines for the experimental programme. The principal test methods and the corresponding material and structural properties reported by Liew [15] are summarised in Table 2.3.

Table 2.3: Main test methods and corresponding standards considered in the experimental programme reported by Liew *et al.* [15] for the material and structural characterisation of additively manufactured composite sandwich structures.

Component	Type of test	Test Standard
Face sheet	Tensile test (nylon)	DIN EN ISO 527–2
	Tensile test (CFRP)	DIN EN ISO 527–4 DIN EN ISO 527–5
	Flexural test (nylon)	DIN EN ISO 178
	Flexural test (CFRP)	DIN EN ISO 14125
	Shear test	ASTM D5379/D5379M
Sandwich core	Shear test	DIN 53 294 ASTM C273/C273M
	Compression test	ASTM C365/C365M
	Tensile test in flatwise plane	DIN 53 292
	Tensile test	ASTM C363/C363M
Sandwich panel	Four-point flexural test	DIN 53 293

At the structural level, the manufacturing-induced features discussed in the previous section introduce additional challenges for material characterisation. In particular, voids, imperfect bonding between deposited beads, and the interaction between sandwich constituents complicate stress transfer and make it more difficult to establish reliable relationships between experimentally measured properties and predictive numerical models. Polyzos *et al.* [12] showed that printed composites may behave as an aggregate of individual beads separated by voids rather than as a perfectly continuous material, while Kubota et al. [20] observed weak fusion between adjacent print paths and increased porosity for certain raster orientations.

Another example of challenge is provided by Liew *et al.* [15], who attempted to determine the stiffness properties of a printed nylon core through four-point flexural tests supported by finite element modelling. However, process limitations of the Markforged system prevented the infill from being printed without roof and floor layers, resulting in specimens with an unavoidable sandwich-like configuration. In addition, printing defects prevented a reliable verification of the estimated core stiffness properties, and the intended material characterisation could not be completed successfully.

Although the core properties could not be determined reliably, the subsequent investigation of the complete sandwich structure still provided valuable insights into its structural behaviour. Flexural bending tests combined with finite element analyses enabled the evaluation of the global response of the sandwich panel, including its flexural and shear

stiffness. Nevertheless, discrepancies remained between the experimental and numerical results, largely due to uncertainties in the material properties of both the printed CFRP face sheets and the nylon core, together with limitations inherent to the printing process. The experimentally derived orthotropic properties of the printed CFRP face sheets, together with the measured flexural and shear stiffness of the sandwich panel, Table 2.4, provides a consolidated view of the material and structural response of the additively manufactured system, as reported by Liew *et al.* [15].

Table 2.4: Summary of material properties and structural stiffness of a Markforged-based CFRP/nylon sandwich system reported by Liew [15] under four-point bending tests.

Component	Property	Method / Basis	Value	Unit
CFRP face sheets	Fibre volume fraction, (ϕ)	Tensile test	0.24	–
		Micromechanics	0.24	–
	$E_{c,1}$	Tensile test	56899	MPa
		Micromechanics	55914	MPa
	$E_{c,2}$	Tensile test	5585	MPa
		Micromechanics	2920	MPa
	$G_{c,12}$	Tensile test	1969	MPa
		Micromechanics	1076	MPa
	$\nu_{c,12}$	Tensile test	0.36	–
		Micromechanics	0.36	–
Full sandwich panel	Average experimental flexural stiffness, (EI_{exp})	Four-point flexural test	21.9	Nm^2
	Standard deviation of (EI_{exp})	Calculated from 15 reported tests	0.6	Nm^2
	Average experimental shear stiffness, (S_{exp})	Four-point flexural test	14626	N
	Standard deviation of (S_{exp})	Calculated from 15 reported tests	428	N

Finally, the reliability of experimentally determined properties also depends on practical aspects of specimen fabrication and testing. Liew [15] highlights the importance of minimising printing defects, printing specimens individually to reduce repeated failures, allowing sufficient cooling time before specimen removal, ensuring careful support removal to prevent damage, and maintaining consistent specimen orientation during testing. Environmental effects must also be considered, since Kubota *et al.* [20] reported that moisture absorption degrades the mechanical properties of the PA-6 matrix. These practical considerations are therefore essential for obtaining consistent and reliable material and structural characterisation data, which are required for meaningful comparison with analytical and numerical models of additively manufactured composite structures.

2.3. Numerical modelling approaches

Finite element analysis (FEA) plays an important role in the study of additively manufactured sandwich structures, as it enables the prediction of structural behaviour and supports the interpretation of experimental results. In the literature, FEA is mainly used to simulate the response under mechanical loading and to estimate stiffness-related properties of printed structures. Although more advanced multi-scale approaches have been proposed, numerical modelling of sandwich structures is still primarily focused on capturing the global mechanical response of the component [12].

Within this context, Liew [15] applied FEA to both the nylon core and the full sandwich structure under four-point bending loading. The numerical framework was based on the modelling strategy proposed by Wolf [23], with refinements aimed at improving the representation of the printed CFRP face sheets, particularly through the incorporation of orthotropic material behaviour and layer orientation effects. However, the author also notes that the predictive capability of the model remained limited, as the results were highly sensitive to the assumed material properties and to simplifications imposed by manufacturing constraints.

For the sandwich core, the numerical model was intended to support the experimental determination of stiffness properties. However, since the experimental characterisation of the core was not successfully completed, the numerical predictions could not be properly validated. As a result, the reliability of the assumed core behaviour remained uncertain, highlighting the limitations of simplified material descriptions for direction-dependent printed polymers.

For the complete sandwich structure, FE simulations were used to reproduce the four-point bending response and compare it with experimental results. Although the global deformation trends were captured, discrepancies between numerical and experimental results were still observed. These differences were mainly attributed to uncertainties in the material properties of the printed CFRP face sheets, the assumed behaviour of the nylon core, and the influence of process-induced variability. This indicates that, despite improvements over previous modelling strategies, accurate prediction of structural response remains strongly dependent on the quality of the input material data.

The importance of accurate material representation is further reinforced in the literature. Mizukami [13] demonstrated that good agreement between experimental and numerical results can be achieved when print-path-dependent anisotropy is explicitly incorporated into the material model, particularly for short carbon fibre-reinforced polymers. Similarly, Polyzos *et al.* [12] showed that the predictive capability of numerical models is highly sensitive to the material data used as input. Models based on properties derived from non-printed materials tend to overestimate strength, whereas those using experimentally characterised printed materials provide more accurate predictions. This is particularly relevant for damage modelling, where the use of realistic material parameters improves agreement between simulations and experiments.

Overall, the literature indicates that FEA is a valuable tool for analysing additively manufactured sandwich structures, but its reliability depends strongly on the quality and representativeness of the material modelling. In particular, the accurate definition of anisotropy, layer-dependent behaviour, and experimentally derived properties is essential for improving predictive capability. For this reason, numerical analyses are most effective when combined with experimental characterisation and when modelling assumptions remain consistent with the actual printed structure [12], [13], [15].

3. EXPERIMENTAL PROGRAMME AND METHODOLOGY

3.1. Experimental Program

3.1.1. Materials

The experimental programme included the characterisation of the two material configurations used in the manufacture of the sandwich structures: Onyx® and Onyx® reinforced with continuous carbon fibre. Mechanical tests were performed to determine the material properties under the same manufacturing conditions adopted throughout this work.

Although Markforged provides mechanical properties for both Onyx® and continuous carbon fibre reinforced parts, the corresponding printing parameters are not fully specified. Since the mechanical response of additively manufactured composites is strongly influenced by the printing process, considerable variations in the reported properties can be found in the literature [24]. Therefore, the material properties were determined experimentally using specimens manufactured with the same equipment, materials and printing parameters adopted for the sandwich specimens.

The resulting mechanical properties were subsequently used to evaluate the structural performance of the sandwich specimens and as input data for the finite element model developed in this dissertation.

3.1.2. Specimen Design and Manufacturing

All specimens used in this work were first designed in SolidWorks according to the dimensions specified by the corresponding testing standards. The CAD models were then imported into the Eiger slicing software, where the printing configuration and reinforcement strategy were defined before fabrication using a Markforged Mark Two 3D printer. The overall workflow adopted in this study is illustrated in **Figure 3.1**.

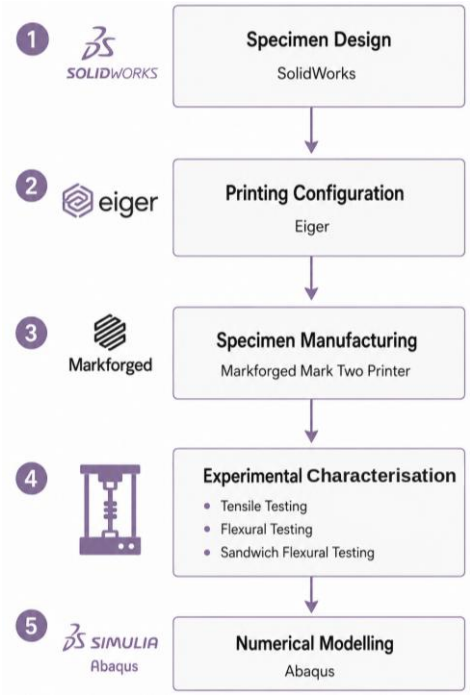


Figure 3.1: Workflow adopted for the design, printing configuration, manufacturing, experimental characterisation and numerical modelling.

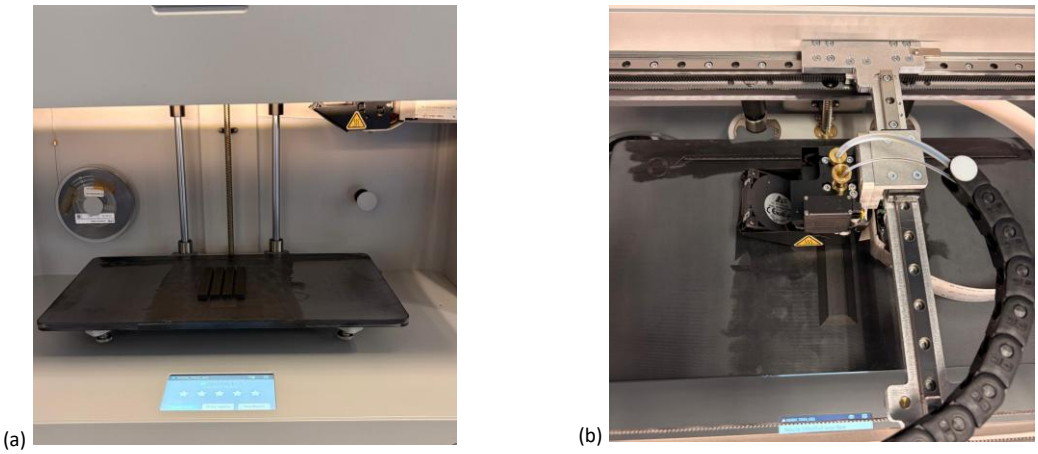


Figure 3.2: Markforged Mark Two printer used to manufacture the specimens: (a) build plate with completed specimens and the touchscreen interface; (b) detail of the print head, showing the plastic and continuous-fibre deposition nozzles.

Although the same manufacturing procedure was followed for all specimens, different internal layer arrangements were adopted according to the specimen configuration. The material characterisation specimens were manufactured either as fully solid Onyx® specimens or as solid specimens reinforced with continuous carbon fibre, whereas the sandwich specimens were produced using a 50% triangular infill to reproduce the intended structural configuration. The corresponding layer arrangements are illustrated in **Figure 3.3**.

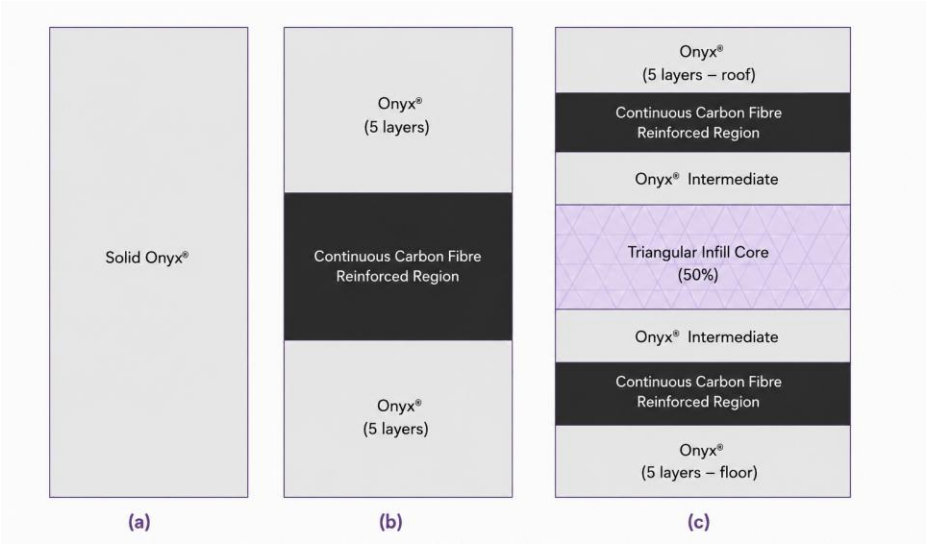


Figure 3.3: Layer arrangement adopted for (a) fully solid Onyx® specimens, (b) continuous carbon fibre reinforced specimens and (c) sandwich specimens.

As shown in **Figure 3.3** the Onyx® specimens were manufactured as fully solid parts. For the continuous carbon fibre reinforced material specimens, the overall specimen geometry was defined by the imported CAD model, while the thickness of the continuous carbon fibre reinforced region was specified in Eiger. The first and last five printed layers remained as Onyx®, forming the external surfaces of the specimen. For the sandwich specimens, the imported CAD model defined the overall specimen geometry, whereas the roof and floor thicknesses together with the thickness of the continuous carbon fibre reinforced region within each face sheet (1.000 mm) were specified by the user. Based on these user-defined parameters, Eiger automatically generated the intermediate Onyx® layers and the core thickness. The resulting nominal cross-section of the sandwich specimens, including the individual layer thicknesses, is detailed in **Table 3.1**.

Table 3.1: Nominal cross-section of the sandwich specimens, as defined in the Eiger slicing software.

Position (top to bottom)	**Material**	**Thickness (mm)**
1	Onyx® (outer)	0.625
2	Continuous carbon fibre-reinforced Onyx® (0°)	1.000
3	Onyx®	0.500
4	Cellular core (50% triangular infill)	4.125
5	Onyx®	0.125
6	Continuous carbon fibre-reinforced Onyx® (0°)	1.000
7	Onyx® (outer)	0.625
Total		**8.000**

Although the internal architectures differed according to the specimen type, the same general printing settings were adopted whenever possible. The printing parameters defined in Eiger for each specimen configuration are summarised in **Table 3.2**.

Table 3.2: Main printing parameters adopted for the manufactured specimens.

Parameter	Material specimens	Sandwich specimens
Printer	Markforged Mark Two	Markforged Mark Two
CAD software	SolidWorks	SolidWorks
Slicing software	Eiger	Eiger
Layer height	0.125 mm	0.125 mm
Infill pattern	Solid	Triangular
Infill density	100%	50%
Wall layers	2	2
Roof/Floor layers	5	5
Fibre orientation	None or 0° *	0°
Fibre pattern Type	Entire group	Entire group
Fibre fill type	Isotropic	Isotropic
Concentric Rings	0	0
Build orientation	0°, 90° or 45°**	0°
* Depending on the specimen type. ** Depending on the specimen configuration		

Representative printing configurations defined in Eiger are presented in **Figure 3.4**. The figure summarises the specimen build orientation, material configuration, layer arrangement and fibre distribution adopted for the different specimen types manufactured in this work.

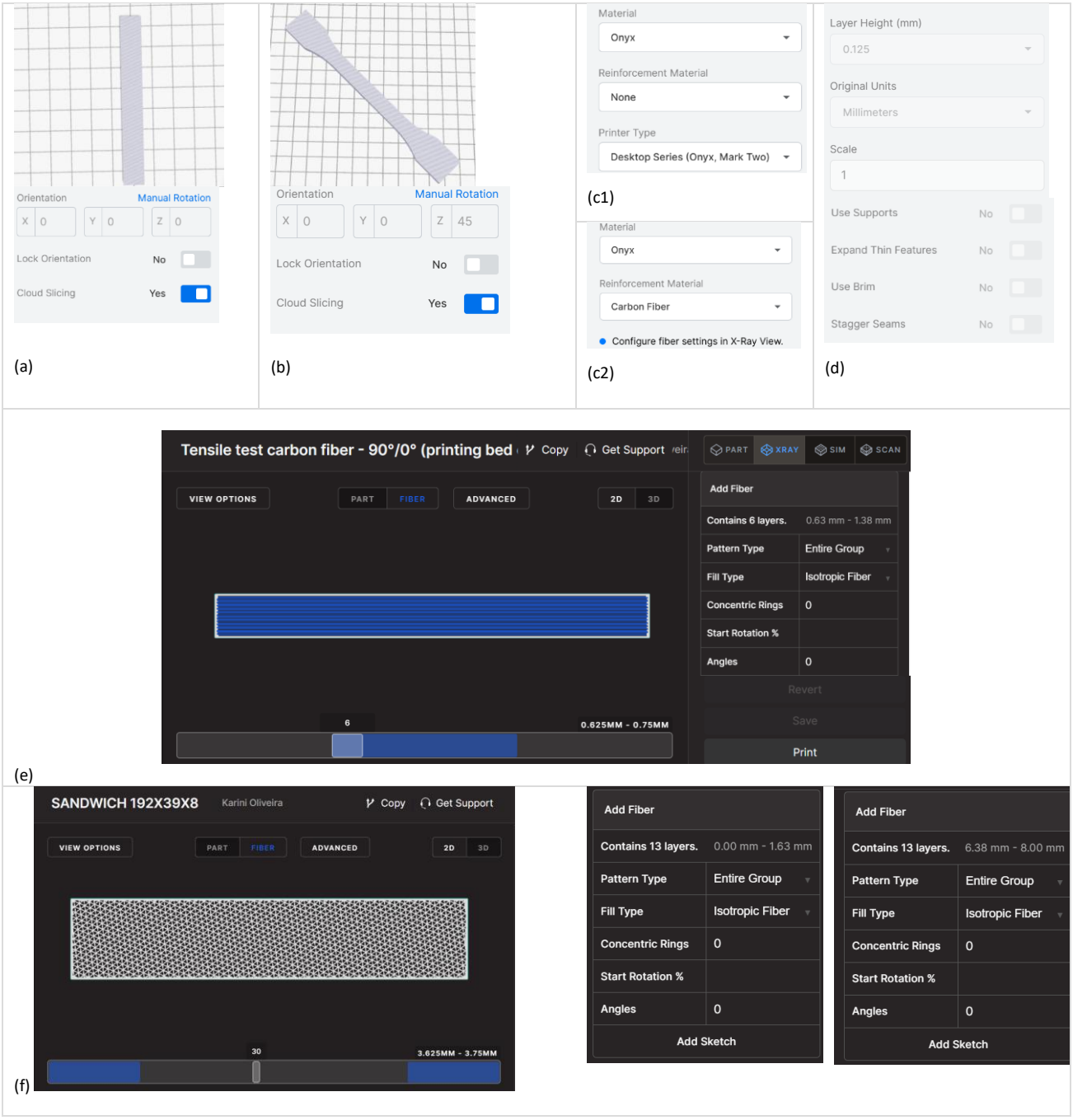


Figure 3.4: Representative Eiger printing configurations showing: (a) specimen orientation for a 0° build orientation; (b) specimen orientation for a 45° build orientation; (c1) Onyx® material configuration; (c2) Onyx® reinforced with continuous carbon fibre and sandwich material configuration; (d) layer configuration; (e) X-ray view and fibre configuration of the continuous carbon fibre reinforced material specimens; and (f) X-ray view and fibre configuration of the sandwich specimens.

3.1.3. Experimental Programme Scope

The experimental programme was designed to characterise the materials and sandwich structures investigated in this work and to provide the experimental data required for the numerical modelling presented in Chapter 5.

Five specimens were initially planned for each experimental configuration. However, due to material availability, a reduced number of specimens was tested in some experimental series. In total, 38 specimens were tested, with a minimum of three specimens evaluated for each series. The exact number of specimens tested for each configuration is indicated in the corresponding experimental sections. Prior to mechanical testing, the dimensions of all specimens were measured and presented in the Annex to verify compliance with the nominal dimensions specified for each test.

The experimental programme focused on the material configurations and build orientations adopted for the manufacture of the sandwich specimens. Consequently, additional specimens required for a complete orthotropic characterisation of the material and the mechanical characterisation of the infill core as an isolated structure were not included within the scope of this work.

3.1.4. Specimen Nomenclature

A systematic nomenclature was adopted to identify the specimens manufactured and tested in this work. This nomenclature is used consistently throughout the dissertation to facilitate the presentation and discussion of the experimental and numerical results.

Table 3.3: Specimen identification system adopted in this work.

Position	Code	Description
1 – Test type	T	Tensile test
	F	Flexural test
	S	Sandwich flexural test
2 – Material	O	Onyx®
	F	Continuous carbon fibre reinforced Onyx®
3 – Fibre orientation	0	Continuous fibres oriented at 0°
	NF	No continuous fibres
4 – Printing bed orientation	0.90	Specimen printed in the 0°/90° orientation
	45.45	Specimen printed in the +45°/−45° orientation

The specimen designation is formed by combining the four elements described in **Table 3.3**. For example, the code T-F-0-45.45 identifies a tensile specimen manufactured in continuous

carbon fibre reinforced Onyx®, with fibres oriented at 0°, printed using a +45°/−45° build orientation.

It should be noted that the Build orientation refers to the orientation of the specimen on the build platform during manufacturing rather than to the raster angle itself. Consequently, specimens printed with a 0°/90° build orientation exhibit a ±45° raster orientation, whereas specimens printed with a +45°/−45° build orientation exhibit a 0°/90° raster orientation. The two printing bed orientations adopted in this work are illustrated in **Figure 3.4** (a) and (b).

3.2. Experimental Equipment

All specimens were designed and prepared at the University of Minho and manufactured using a Markforged Mark Two 3D printer at the Instituto de Soldadura e Qualidade (ISQ). All mechanical tests presented in this work were performed at the Structural Laboratory of the University of Minho using the experimental equipment summarised in **Table 3.4**, which includes the main testing, deformation measurement and data acquisition equipment used throughout the experimental programme, together with the relevant specifications of the strain gauges used for the sandwich flexural tests. The corresponding experimental setup is illustrated in **Figure 3.5**.

Table 3.4: Experimental equipment used for the mechanical characterisation of the printed specimens.

Equipment	Model / Description
Universal testing machine	MTS Exceed E45.105, tabletop-type universal testing machine with a single test zone and a maximum rated force capacity of 100 kN. Operating speed range: 0.001–508 mm/min; position resolution: 0.000041 mm; vertical test space (crosshead travel): 1000 mm; space between columns: 340 mm.
Load cell	100 kN
Video extensometer	MTS Advantage XT-205b, with a maximum transverse gauge length of 63 mm and a typical extension resolution of 0.25 µm. Capable of measuring axial strains on specimens as narrow as 1.4 mm and transverse strains on specimens with a minimum width of 6.4 mm. Maximum tracking speed: 350 mm/min; optical field of view (FOV): 86 × 72 mm.
Test control software	MTS TestSuite TWE Elite
Strain acquisition software	MTS AVX Software
Strain gauge	HBM 3/120ELY91-3/120E; nominal resistance: 120 Ω; gauge factor: 2.02 ± 1.0%

(a) 



Figure 3.5: Experimental equipment used throughout the experimental programme: (a) MTS Exceed E45.105 universal testing machine; (b) MTS Advantage (AVX) video extensometer system.

3.3. Tensile Test of Printed Onyx® Specimens

The mechanical behaviour of the printed Onyx® material under tensile loading was characterised according to ISO 527-2:2012.

Dumbbell-shaped Type 1B specimens were manufactured according to the dimensions specified in the standard. The specimen geometry is presented in **Figure 3.6**. Two printing bed orientations (0°/90° and 45°/-45°) were considered. The number of specimens tested for each configuration is summarised in **Table 3.5**.

Table 3.5: Summary of the Onyx® tensile specimens tested.

Build orientation	Specimen identification	Number of specimens
0°/90°	T-O-NF-0.90	4
45°/-45°	T-O-NF-45.45	5

Figure 3.6: Geometry and dimensions of the Onyx® tensile specimen.

The tensile tests were performed using the experimental equipment described in section 3.2. The corresponding experimental setup is shown in **Figure 3.7**.



Figure 3.7: Experimental setup used for the tensile tests.

The specimens were tested under displacement control at a crosshead speed of 1.0 mm/min, without the application of a preload. Strain was measured using two virtual extensometers with a gauge length of 50 mm defined in the MTS AVX Software, based on four reference marks applied to the specimen surface. During the tests, the applied force, crosshead displacement and specimen strain were continuously recorded. The acquired data were subsequently processed to obtain the stress–strain curves presented and discussed in Chapter 4.

3.4. Tensile Test of Printed Carbon Fibre Reinforced Onyx® Specimens

The tensile behaviour of the continuous carbon fibre reinforced Onyx® material was characterised according to ISO 527-4:2023.

Rectangular Type 2 specimens with dimensions of 250 × 15 × 1 mm were manufactured according to ISO 527-5:2009. Only the 0°/90° printing bed orientation was considered in this study. Specimens with a 45°/-45° printing bed orientation were not manufactured because their overall dimensions exceeded the available build volume of the Markforged Mark Two printer. The number of specimens tested is summarised in **Table 3.6**.

Table 3.6: Summary of the continuous carbon fibre reinforced Onyx® tensile specimens tested.

Printing bed orientation	Specimen identification	Number of specimens
0°/90°	T-F-0-0.90	7

The tensile tests were performed using the experimental equipment described in section 3.2. The corresponding experimental setup is shown in **Figure 3.8.**

(a)





Figure 3.8: Tensile test specimens: (a) specimen without tabs, showing premature failure in the gripping region; (b) specimen with bonded tabs adopted for the final testing procedure.

Preliminary tensile tests performed without tabs resulted in premature failure in the gripping region. Therefore, tabs were bonded to the specimens to ensure failure occurred within the gauge section, in accordance with ISO 527-5:2009. The two configurations are shown in **Figure 3.8**.

The specimens were tested under displacement control at a crosshead speed of 5.0 mm/min, without the application of a preload, strain was measured using two virtual extensometers with a gauge length of 50 mm defined in the MTS AVX Software, based on four reference marks applied to the specimen surface. During the tests, the applied force, crosshead displacement and specimen strain were continuously recorded.

3.5. Flexural Test of Printed Onyx® Specimens

The flexural behaviour of the printed Onyx® material was characterised according to BS EN ISO 178:2019 using three-point bending tests.

Rectangular specimens with nominal dimensions of 80 mm × 10 mm × 4 mm were manufactured in accordance with the standard. Two printing bed orientations (0°/90° and 45°/-45°) were investigated to evaluate the influence of the printing orientation on the flexural behaviour of the material. The specimen configurations and number of specimens are summarised in **Table 3.7**.

Table 3.7: Summary of the Onyx® flexural tested specimens.

Printing bed orientation	Specimen identification	Number of specimens
0°/90°	F-O-NF-0.90	5
45°/-45°	F-O-NF-45.45	4

The flexural tests were performed using the experimental equipment described in Section 3.2. The experimental setup is presented in **Figure 3.9**.

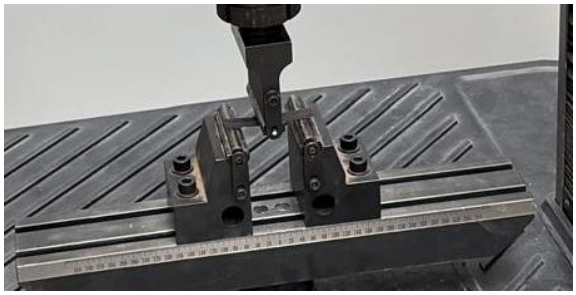


Figure 3.9: Experimental setup used for the three-point bending tests of Onyx® specimens.

The specimens were tested under displacement control in a three-point bending configuration with a 64 mm support span and a crosshead speed of 5.0 mm/min, without the application of a preload. During the tests, the applied force and crosshead displacement were continuously recorded.

3.6. Flexural Test of Printed Continuous Carbon Fibre Reinforced Onyx® Specimens

The flexural behaviour of the continuous carbon fibre reinforced Onyx® material was characterised according to BS EN ISO 14125:1998 + A1:2011 using three-point bending tests.

Rectangular specimens with nominal dimensions of 100 mm × 15 mm × 2 mm were manufactured in accordance with the standard. Two printing bed orientations (0°/90° and 45°/-45°) were investigated to evaluate the influence of the printing bed orientation on the flexural behaviour of the material. Five specimens were tested for the 0°/90° orientation and five specimens for the 45°/-45° orientation. The specimen configurations are summarised in **Table 3.8**

Table 3.8: Summary of the continuous carbon fibre reinforced Onyx® flexural test specimens.

Printing bed orientation	Specimen identification	Number of specimens
0°/90°	F-F-0-0.90	5
45°/-45°	F-F-0-45.45	5

The flexural tests were performed using the experimental equipment described in Section 3.2 . The experimental setup is presented in **Figure 3.10**.



Figure 3.10: Experimental setup used for the three-point bending tests of Carbon fibre-reinforced Onyx® specimens.

The specimens were tested under displacement control in a three-point bending configuration with an 80 mm support span and a crosshead speed of 2.0 mm/min, without the application of a preload. During the tests, the applied force and crosshead displacement were continuously recorded.

3.7. Four-Point Bending Test of Sandwich Specimens

The structural behaviour of the manufactured sandwich specimens under flexural loading was evaluated by means of four-point bending tests conducted in accordance with DIN 53 293. The test was performed to characterise the structural flexural response of the sandwich specimens and to provide experimental data for the validation of the numerical model developed in this work. The specimen configuration is summarised in **Table 3.9**.

Table 3.9: Summary of the sandwich specimens tested.

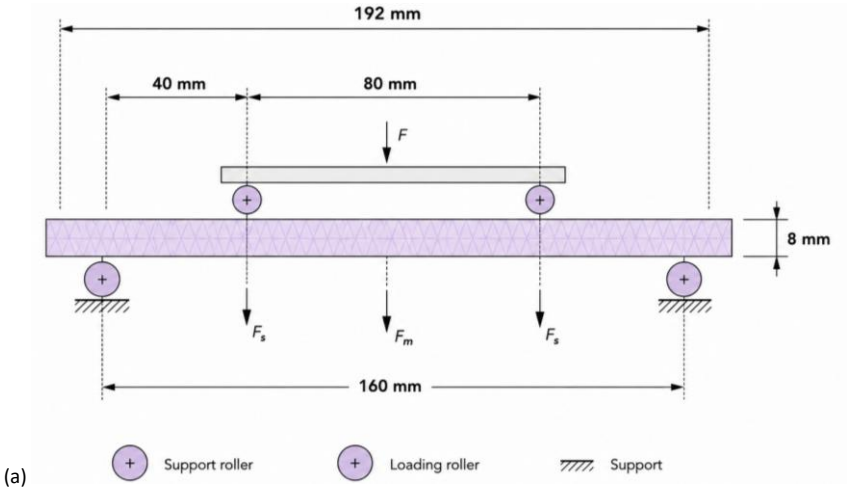
Specimen configuration	Specimen identification	Number of specimens
Sandwich structure	S-F-0-0.90	3

A white speckle pattern was applied to the lateral surface of the sandwich specimens to enable optical tracking of the specimen deformation using the video extensometer and video extensometry software. In addition, a strain gauge was bonded to the middle of the bottom surface of each specimen to measure the local longitudinal strain during bending. An example of the speckle pattern applied to the specimen surface is shown in **Figure 3.11**.

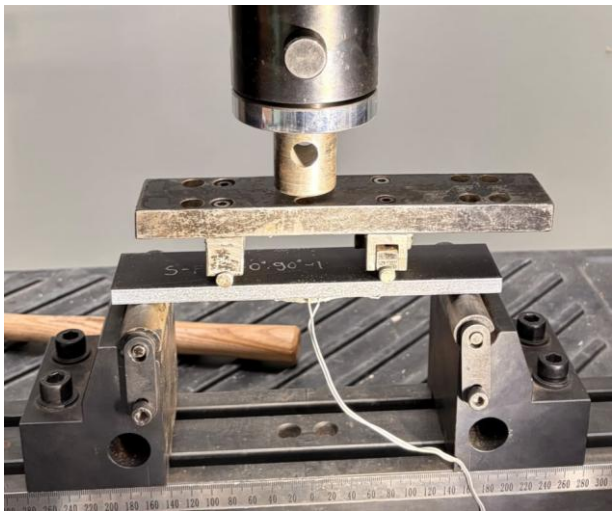


Figure 3.11: Sandwich specimen prepared for the four-point bending test, showing the speckle pattern applied to the lateral surface for optical deformation measurement.

The flexural tests were performed using the experimental equipment described in section 3.2. The experimental setup is presented in **Figure 3.12**, including a schematic representation of the loading configuration and the corresponding experimental arrangement.



(a)



(b)

Figure 3.12: Four-point bending test setup for the sandwich specimens: (a) schematic representation of the loading configuration according to DIN 53 293; (b) experimental setup used in the present study.

The specimens were positioned on the lower support rollers and carefully aligned with the loading rollers to ensure a uniform distribution of the applied load. The support and loading spans were set to 160 mm and 80 mm, respectively. The loading and support rollers had a diameter of 8 mm, complying with the requirements of the standard. A preload of 1 N was applied before each test to ensure full contact between the rollers and the specimen. The tests were conducted under displacement control at a crosshead speed of 2 mm/min. During testing, the applied load, crosshead displacement and strain measurements were continuously recorded.

4. Experimental Results and Discussion

4.1. Tensile Behaviour of Printed Onyx® Specimens

The tensile behaviour of the printed Onyx® specimens was evaluated by means of tensile tests conducted according to ISO 527-2:2012. The manufactured specimens presented good printing quality and surface finish, with no visible defects or printing imperfections observed prior to testing, as shown in **Figure 4.1**. No noticeable differences were identified between the two printing bed orientations.

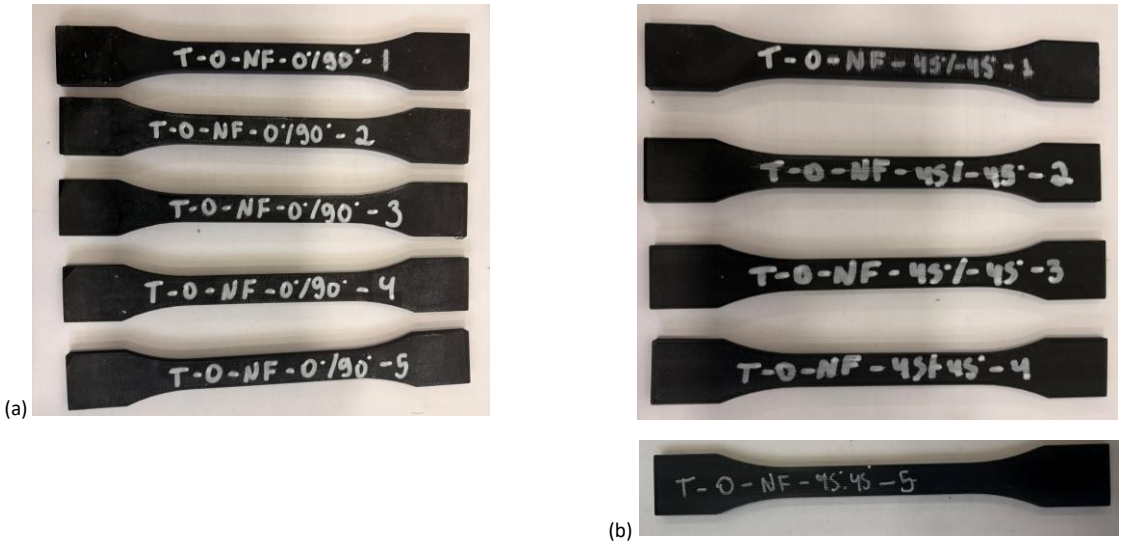


Figure 4.1: Onyx® tensile specimens manufactured for testing: (a) 0°/90° printing bed orientation; (b) 45°/−45° printing bed orientation.

Fracture consistently occurred within the reduced gauge section of the specimens, close to the transition with the upper grip region. The specimens exhibited noticeable plastic deformation before fracture, followed by a sudden loss of load-carrying capacity. Distinct fracture patterns were observed for the two printing bed orientations. Specimens printed with the 0°/90° printing bed orientation (45° raster angle) exhibited an inclined fracture surface of approximately 45°, whereas those printed with the 45°/−45° printing bed orientation (90° raster angle) fractured almost perpendicular to the loading direction. The specimen after

failure and close-up views of the fracture regions are presented in **Figure 4.2** and **Figure 4.3** , highlighting the distinct fracture surfaces observed for the two printing bed orientations.

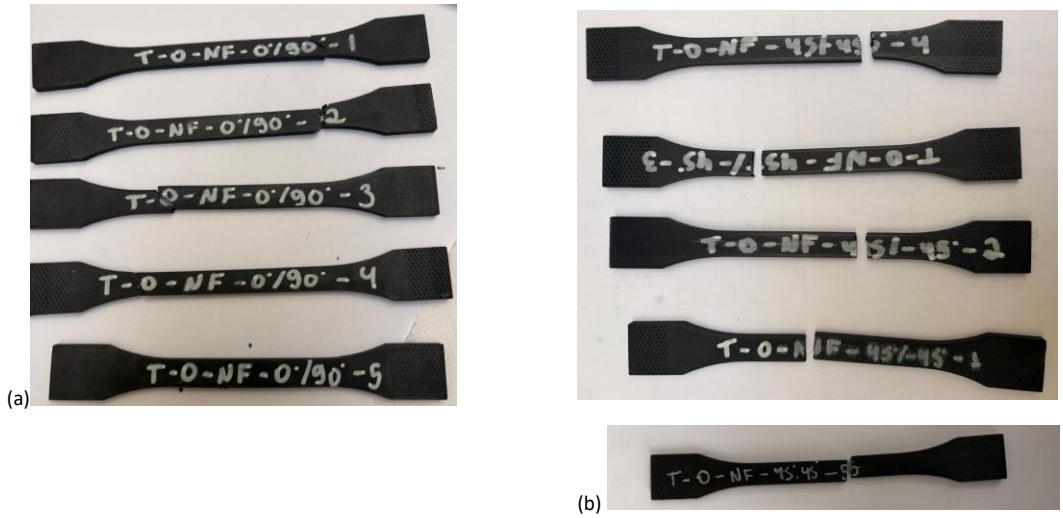


Figure 4.2: Onyx® tensile specimens after testing: (a) 0°/90° printing bed orientation; (b) 45°/−45° printing bed orientation.

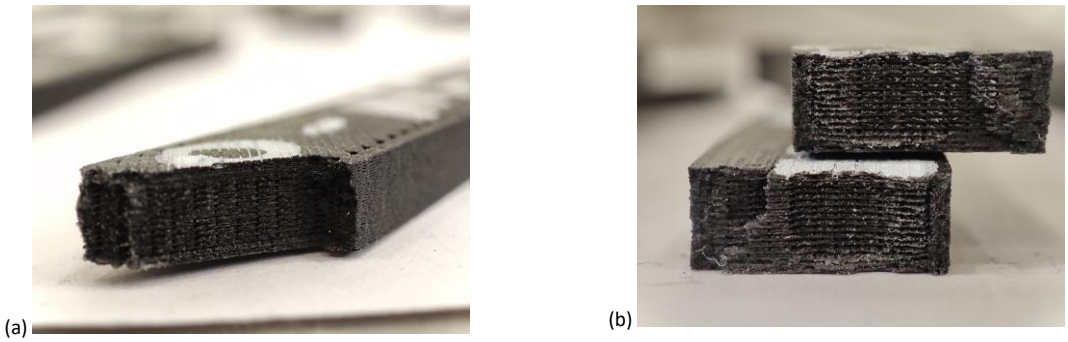


Figure 4.3: Close-up views of the fracture regions of the Onyx® tensile specimens: (a) 0°/90° printing bed orientation; (b) 45°/−45° printing bed orientation.

The engineering stress–strain curves obtained from the valid specimens are presented in **Figure 4.4**. The 0°/90° specimens showed generally similar tensile behaviour, although specimen 2 exhibited a lower tensile strength than the remaining valid specimens. The 45°/−45° specimens showed a more consistent response, with the valid specimens exhibiting similar stress–strain behaviour. In both printing orientations, an initial linear elastic region was observed, followed by a gradual transition to nonlinear behaviour before fracture. No distinct yield point was identified, indicating a progressive transition from elastic to plastic deformation. The 0°/90° specimens exhibited considerably higher strain at failure, reaching an average value of approximately 36%, whereas the 45°/−45° specimens fractured at an average strain of approximately 19%. In contrast, the tensile strength values were of the same

order for both orientations, indicating that the printing bed orientation had a limited influence on tensile strength but a more pronounced effect on stiffness and deformation capacity.

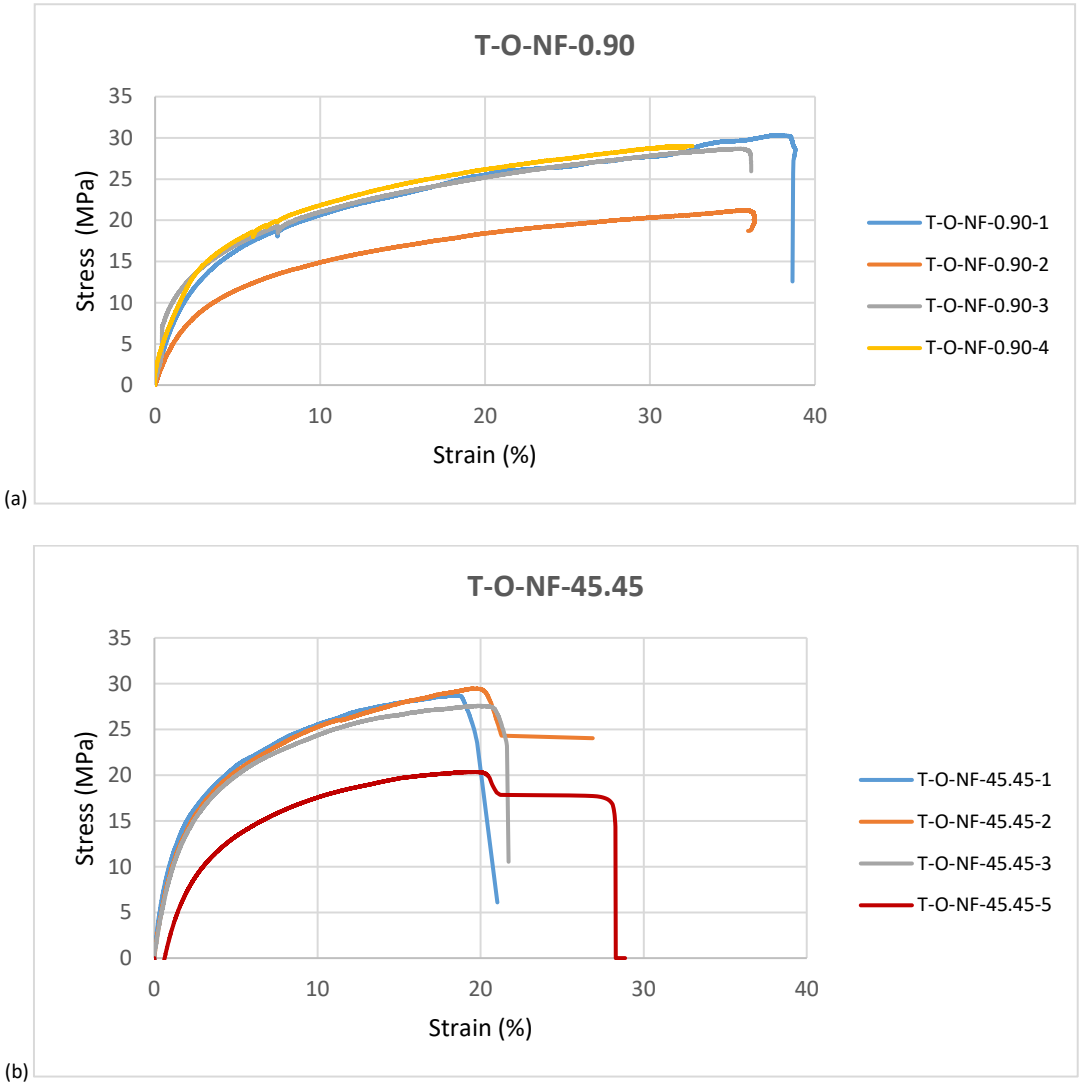


Figure 4.4: Engineering stress–strain curves obtained from the tensile tests of printed Onyx® specimens: (a) 0°/90° printing bed orientation; (b) 45°/−45° printing bed orientation.

For the 0°/90° configuration, specimen 5 was not tested due to technical issues. For the 45°/−45° configuration, specimen 4 was tested but its results were discarded due to technical issues. Therefore, the reported average and standard deviation values are based on four valid specimens for each printing bed orientation.

The average tensile strength obtained for the 0°/90° and 45°/−45° printing bed orientations was 27.47 ± 4.24 MPa and 26.40 ± 3.64 MPa, respectively, indicating only a minor influence of the printing bed orientation on the ultimate tensile strength. In contrast, the tensile modulus increased from 0.726 ± 0.110 GPa for the 0°/90° specimens to 1.187 ± 0.295 GPa for the

45°/−45° specimens, while the strain at failure decreased from 36.32 ± 1.00% to 19.37 ± 0.60%. These results indicate that the 45°/−45° printing bed orientation produced stiffer specimens with lower deformation capacity, whereas the 0°/90° orientation allowed substantially larger deformations before fracture.

The tensile strengths obtained in this work were lower than the 37 MPa reported by Markforged for Onyx®, as shown in **Table 2.1**. However, direct comparison should be made with caution, as the manufacturer does not disclose all processing parameters used to obtain the reported values. Furthermore, previous studies have reported considerable variability in the mechanical properties of printed Onyx® due to differences in manufacturing and testing conditions. Batley *et al.* [24], for example, reported an average tensile strength of 44.17 MPa and an elastic modulus of 1.01 GPa, demonstrating that significant differences may exist even among studies using the same material. Therefore, the discrepancies observed in the present work are likely associated with variations in processing parameters and experimental conditions rather than the intrinsic properties of Onyx® alone.

Table 4.1: Mechanical properties obtained from the tensile tests of printed Onyx® specimens.

T-O-NF				
Printing bed Orientation	**Samples**	**Tensile Strength (MPa)**	**Tensile Strain (%)**	**Tensile Modulus (GPa)**
0°/90°	1	30.29	37.69	0.761
	2	21.18	35.66	0.592
	3	28.67	35.50	0.697
	4	29.71	36.45	0.855
	5	*	*	*
	Average	**27.47**	**36.32**	**0.726**
	Standard deviations	**4.24**	**1.00**	**0.110**
45°/-45°	1	28.73	18.49	1.481
	2	29.47	19.60	1.072
	3	27.58	19.82	1.077
	4	25.87	**	**
	5	20.36	19.57	1.120
	Average	**26.40**	**19.37**	**1.187**
	Standard deviations	**3.64**	**0.60**	**0.295**

Notes:
*Sample not tested due to technical issues.
**Results discarded due to technical issues.

4.2. Tensile Behaviour of Printed Carbon Fibre-Reinforced Onyx® Specimens

The tensile properties were calculated in accordance with ISO 527-4:2023 for fibre-reinforced plastic composites. The manufactured specimens 1–5 generally presented good printing quality, although some specimens exhibited slight curvature along the lateral edges. Overall, these specimens were considered to have acceptable manufacturing quality despite these minor imperfections. A second group of specimens 6–8 presented more pronounced manufacturing imperfections, including bubbles in the outer layers and local curvature of the continuous carbon fibre. These differences in manufacturing quality are illustrated in **Figure 4.5** and **Figure 4.6**.

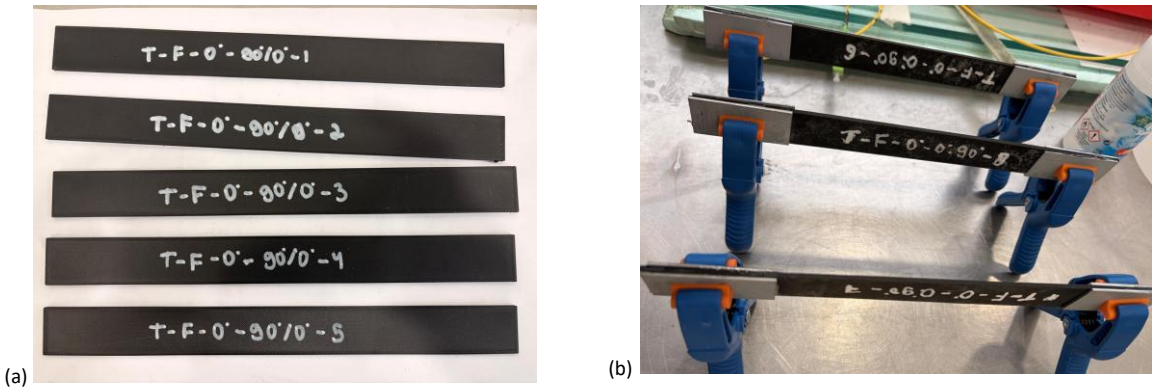


Figure 4.5: Carbon fibre-reinforced Onyx® tensile specimens before testing: (a) specimens 1–5; (b) specimens 6–8.

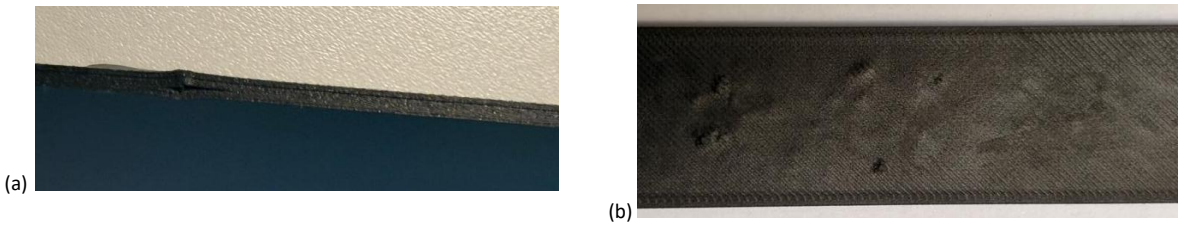
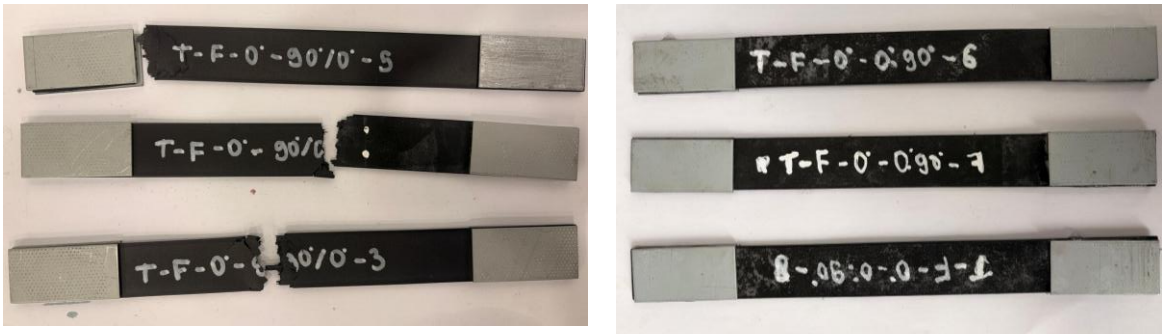


Figure 4.6: Close-up views of the carbon fibre-reinforced Onyx® tensile specimens before testing, highlighting the observed manufacturing imperfections: (a) slight lateral curvature; (b) bubbles in the outer layer and curvature of the continuous carbon fibre.

The specimens 6–8 were produced when the carbon fibre supply was near the end of the spool. Although the printer indicated that sufficient material remained, these were the final specimens produced before the carbon fibre was depleted. The relationship between the

remaining material supply and the observed manufacturing imperfections was not investigated, as this was outside the scope of the present study.

All tensile tests were successfully conducted. Seven specimens were included in the final experimental results. Specimen 1 was tested without tabs, and its results were retained, while specimen 2 was excluded from the experimental dataset due to technical problems during testing. The specimens with fewer manufacturing imperfections exhibited a clear fracture approximately in the middle of the gauge section, with the fracture occurring approximately perpendicular to the loading direction. In contrast, specimens 6–8 did not exhibit a complete visible fracture. Nevertheless, a reduction in load-carrying resistance was observed during testing, after which the machine stopped the test.



(a) (b)

Figure 4.7: Carbon fibre-reinforced Onyx® tensile specimens after testing: (a) specimens 3–5; (b) specimens 6–8.

A close-up view of the fracture region of some specimens is presented in **Figure 4.8**, providing a more detailed view of the failure region observed during the tensile test.

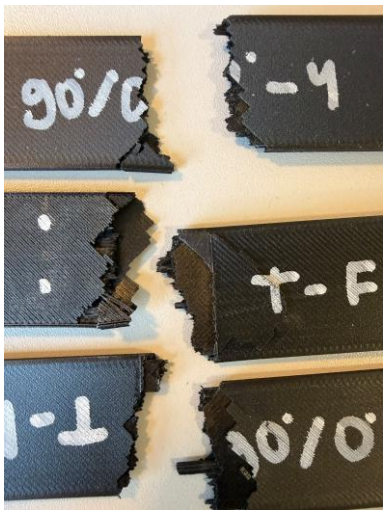


Figure 4.8: Close-up view of the fracture region of carbon fibre-reinforced Onyx® tensile.

The engineering stress–strain curves obtained from the tensile tests are presented in **Figure 4.9**. The specimens with comparatively better manufacturing quality, namely specimens 1, 3, 4 and 5, exhibited a similar overall response, with an approximately linear initial region followed by a progressive increase in stress until reaching the maximum tensile strength. Some local irregularities and small load drops were observed in the curves, particularly at higher strain levels, which may be associated with progressive damage within the reinforced material before final failure. These specimens exhibited visible fracture at tensile strains between approximately 1.3% and 1.6%.

In contrast, specimens 6–8 exhibited a substantially different response. Their stress–strain curves reached considerably lower maximum stress levels and showed a progressive reduction in load-carrying capacity before the tests were stopped. The difference in response between the two groups is particularly relevant when considering the manufacturing imperfections identified in specimens 6–8.

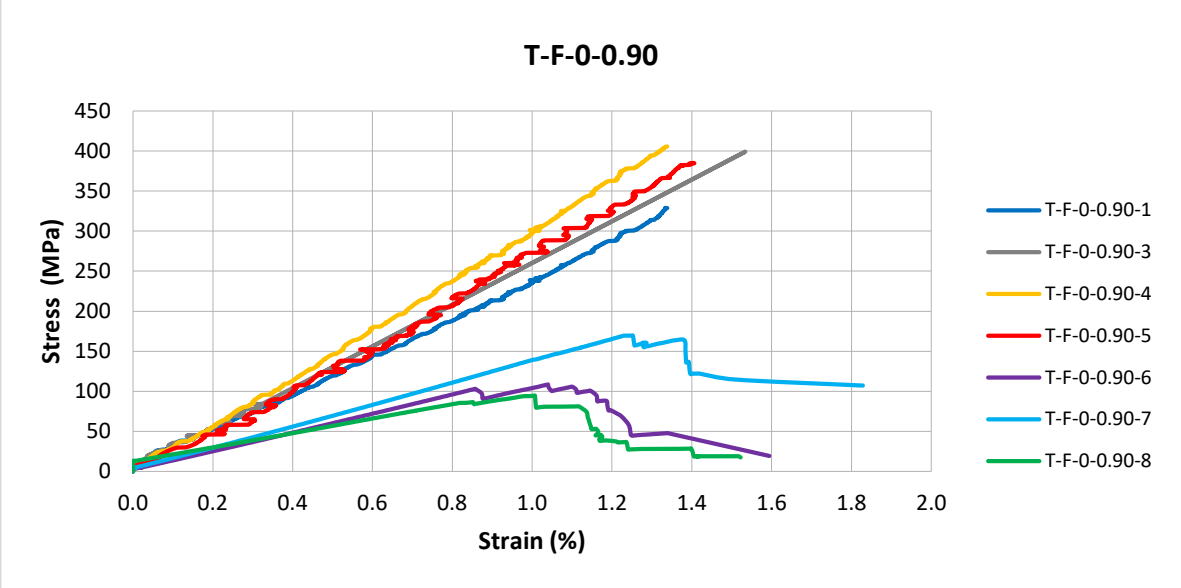


Figure 4.9: Engineering stress–strain curves obtained from the tensile tests of carbon fibre-reinforced Onyx® specimens.

The tensile strength, tensile strain and tensile modulus obtained from the tests are summarised in **Table 4.2**. For specimens 1, 3–5, the average tensile strength was approximately 347.42 MPa, with a standard deviation of 61 MPa. The corresponding average tensile modulus was 23.41 GPa, while the average tensile strain was approximately 1.41%. The relatively small standard deviation in strain (0.12%) indicates consistent deformation behaviour among these specimens.

For specimens 6–8, the average maximum tensile stress was approximately 124.30 MPa, corresponding to a reduction of approximately 64% compared with specimens 1, 3–5. Their average tensile modulus was approximately 11.09 GPa, approximately 53% lower than that of the first group. The average tensile strain reached at the end of the tests was approximately 1.10%. These results indicate a substantial reduction in tensile performance for the specimens exhibiting more pronounced manufacturing imperfections.

Table 4.2: Tensile properties obtained for the carbon fibre-reinforced Onyx® specimens according to manufacturing condition.

T-F-0-0.90			
Specimen	**Tensile strength (MPa)**	**Tensile strain (%)**	**Tensile modulus (GPa)**
1	328.96 *	1.58 *	20.86 *
2	**	**	**
3	269.74	1.34	24.58
4	405.81	1.33	26.02
5	385.15	1.40	22.17
Average (specimens 1, 3–5)	**347.42**	**1.41**	**23.41**
Standard deviation (specimens 1, 3–5)	**61.13**	**0.12**	**2.33**
6	108.53	1.04	11.40
7	169.68	1.25	12.88
8	94.67	1.00	9.00
Average (specimens 6–8)	**124.30**	**1.10**	**11.09**
Standard deviation (specimens 6–8)	**39.91**	**0.13**	**1.96**
Average (all specimens)	**251.79**	**1.28**	**18.08**
Standard deviation (all specimens)	**128.93**	**0.20**	**6.96**

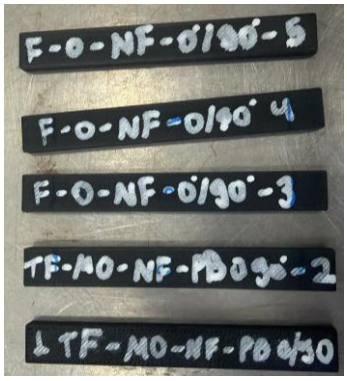
Notes:
* Specimen 1 was tested without tabs.
** Specimen 2 was excluded from the experimental results due to technical problems during testing.

The observed difference between the two groups suggests that the manufacturing condition of the specimens had a significant influence on their measured tensile response. However, because the effect of the carbon fibre supply condition and the observed manufacturing imperfections was not investigated independently, a direct causal relationship cannot be established within the scope of the present study.

4.3. Flexural Behaviour of Printed Onyx® Specimens

The manufactured Onyx® specimens generally presented good printing quality for both printing bed orientations considered. No significant surface defects or differences in

manufacturing quality were observed between the specimens. The specimens before testing are presented in **Figure 4.10**.

(a) 

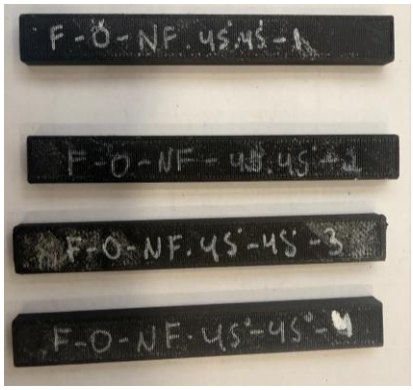
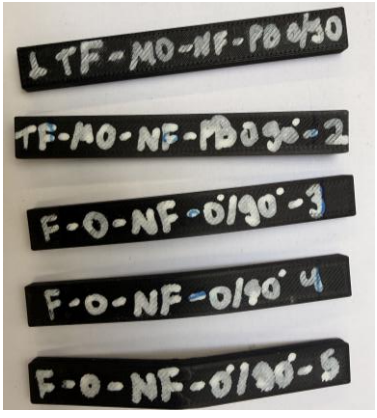
(b) 

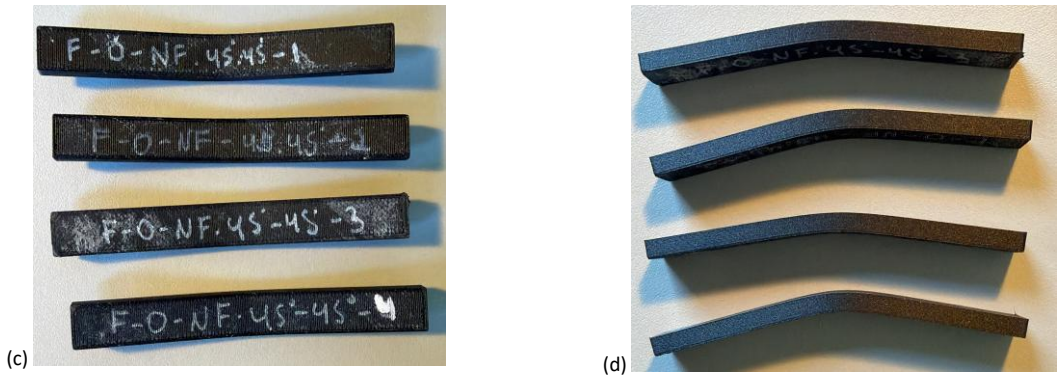
Figure 4.10: Onyx® flexural specimens before testing: (a) 0°/90° printing bed orientation; (b) 45°/−45° printing bed orientation.

The flexural tests were conducted on five specimens with a 0°/90° printing bed orientation and four specimens with a 45°/−45° printing bed orientation. In contrast to the tensile tests, none of the specimens exhibited complete fracture during the flexural tests. The specimens underwent substantial deformation while remaining intact, and after unloading they showed considerable recovery towards their original shape.

The post-test condition of the specimens is shown in **Figure 4.11**. The absence of complete fracture and the substantial deformation observed during testing are evident in the photographs.

(a) 

(b) 



(c) (d)

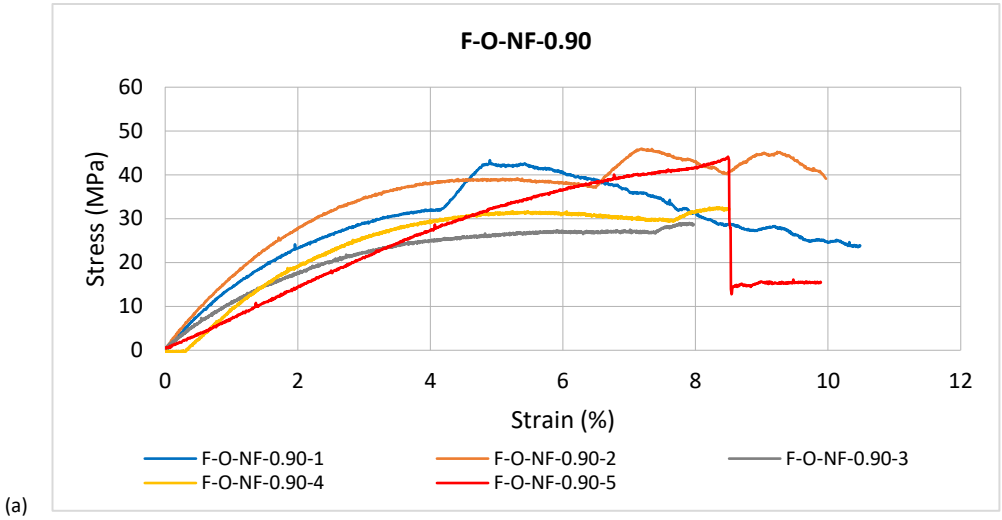
Figure 4.11: Onyx® flexural specimens after testing: (a) front view of specimens with 0°/90° printing bed orientation; (b) lateral view of the same specimens; (c) front view of specimens with 45°/−45° printing bed orientation; (d) lateral view of the same specimens.

At higher deformation levels, the specimens began to move out of the support region, resulting in a loss of stable contact with the supports. This behaviour was accompanied by irregularities and sudden changes in the recorded stress–strain response. An example of the specimen displacement from the supports is shown in **Figure 4.12**

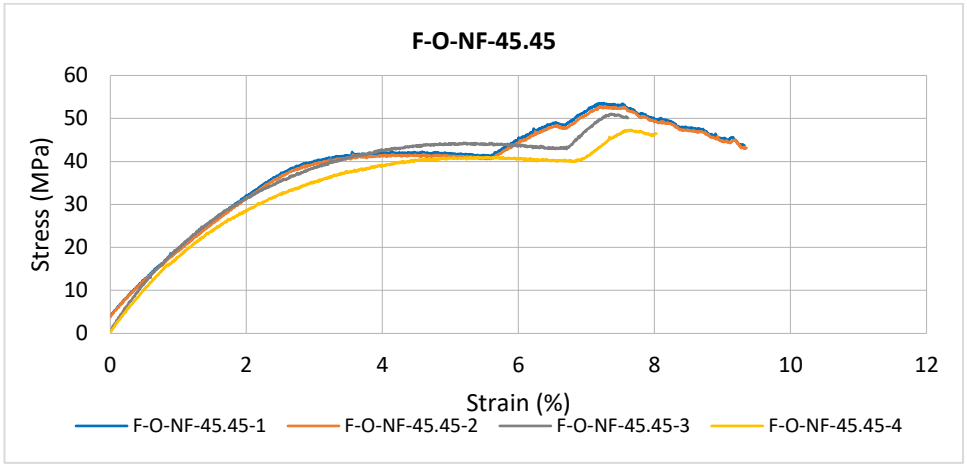


Figure 4.12: Onyx® flexural specimen during testing, showing displacement from the supports at large deformation.

The flexural stress–strain curves obtained for the two printing bed orientations are presented in **Figure 4.13**. Both configurations showed an initially linear response, corresponding to the elastic behaviour of the material. As the deformation increased, the curves gradually became nonlinear. The 45°/−45° specimens showed a steeper initial response than the 0°/90° specimens, which is consistent with the higher flexural modulus obtained for this configuration.



(a)



(b)

Figure 4.13: Engineering stress–strain curves obtained from the flexural tests of Onyx® specimens: (a) 0°/90° printing bed orientation; (b) 45°/−45° printing bed orientation.

As the specimens did not exhibit complete fracture, the flexural stress and corresponding strain at the selected maximum point were determined from the stable portion of the curves, immediately before the onset of the irregular response associated with the displacement from the supports. The procedure used to determine these values is illustrated in **Figure 4.14** for a representative specimen.

These values were calculated in accordance with BS EN ISO 178:2019, which assumes a constant support span between the loading and support points. Since the specimens displaced from the supports as they deformed, the effective span changed during testing; the reported maximum flexural stress and corresponding strain, based on the initial test geometry, should therefore be interpreted with caution.

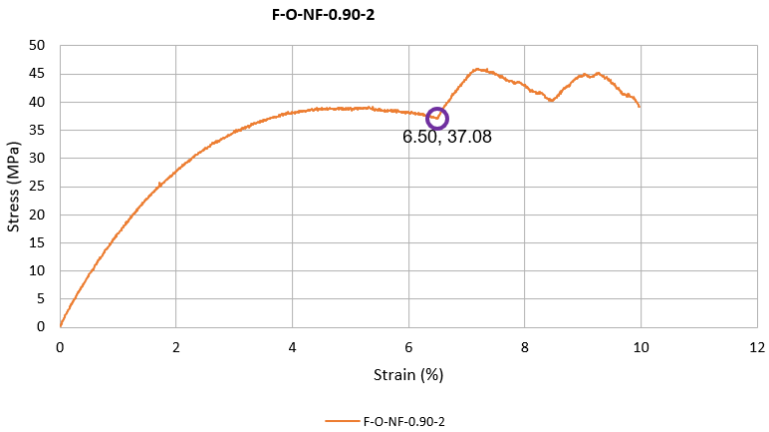


Figure 4.14: Determination of the maximum flexural stress and corresponding strain from a representative Onyx® specimen, based on the stable portion of the stress–strain curve.

For the 0°/90° configuration, five specimens were tested; however, specimen 5 was excluded from the calculation of the average and standard deviation due to its different printing parameters. Therefore, the reported average and standard deviation for this configuration are based on specimens 1–4. The flexural properties obtained for both printing bed orientations are presented in **Table 4.3.**

Table 4.3: Flexural properties obtained for the Onyx® specimens according to printing bed orientation.

F-O-NF				
Printing bed Orientation	**Sample**	**Flexural strength (MPa)**	**Flexural Strain**	**Flexural Modulus (GPa)**
0°/90°	1	32.08	4.12	1.82
	2	37.36	6.43	1.88
	3	37.08	7.91	1.18
	4	28.81	7.94	1.28
	5	41.03*	7.69*	0.63*
	Average	**33.83**	**6.60**	**1.54**
	Standard deviations	**4.13**	**1.80**	**0.36**
45°/-45°	1	41.28	5.59	1.66
	2	43.62	5.96	1.64
	3	44.12	5.27	2.35
	4	40.18	6.52	2.18
	Average	**42.30**	**5.84**	**1.96**
	Standard deviations	**1.88**	**0.54**	**0.36**

Note:
*Specimen 5 was manufactured using different printing parameters and was therefore excluded from the calculation of the average and standard deviation.

The 45°/−45° specimens exhibited higher flexural strength and stiffness than the 0°/90° specimens. The average flexural strength increased from 33.83 MPa for the 0°/90° configuration to 42.30 MPa for the 45°/−45° configuration, while the corresponding flexural modulus increased from 1.54 GPa to 1.96 GPa. These results indicate that the printing bed orientation influenced both the strength and stiffness of the Onyx® specimens under flexural loading.

The average flexural strain at the selected maximum stress was 6.60% for the 0°/90° specimens and 5.84% for the 45°/−45° specimens. Thus, the 45°/−45° configuration exhibited a lower strain at the selected maximum flexural stress despite its higher flexural strength and stiffness.

The flexural strength showed relatively good repeatability for both configurations, with standard deviations of 4.13 MPa for the 0°/90° specimens and 1.88 MPa for the 45°/−45° specimens. The flexural strain presented standard deviations of 1.80% and 0.54%, respectively, while the flexural modulus showed standard deviations of 0.36 GPa for both configurations.

For reference, Markforged reports a flexural strength of 71 MPa and a flexural modulus of 3.0 GPa for Onyx® under the manufacturer-reported test conditions. The values obtained in the present study were lower than the manufacturer-reported values for both printing orientations. These values are considered reference values, as the manufacturing and testing conditions used by the manufacturer may differ from those adopted in the present study.

4.4. Flexural Behaviour of Printed Carbon Fibre-Reinforced Onyx® Specimens

The manufactured carbon fibre-reinforced Onyx® specimens generally presented good printing quality for both printing bed orientations. No significant surface defects or differences in manufacturing quality were observed between the specimens. One exception was the specimen F-F-0-0.90-1, which was produced with four floor layers instead of the five layers specified for the remaining specimens. The specimens before testing are presented in **Figure 4.15**.

(a) 

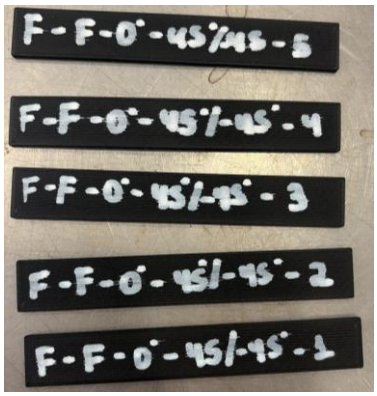
(b) 

Figure 4.15: Carbon fibre-reinforced Onyx® flexural specimens before testing: (a) 0°/90° printing bed orientation; (b) 45°/−45° printing bed orientation.

As observed in the flexural tests of the Onyx® specimens, none of the specimens exhibited complete fracture during the tests. The specimens underwent substantial deformation while remaining intact. Also, it was noticed that the carbon fibre-reinforced specimens progressively moved out of their position on the supports at higher deformation levels. This resulted in irregularities and sudden changes in the recorded stress–strain response. An example of this behaviour is shown in **Figure 4.16**. The post-test condition of the specimens is presented in **Figure 4.17**.

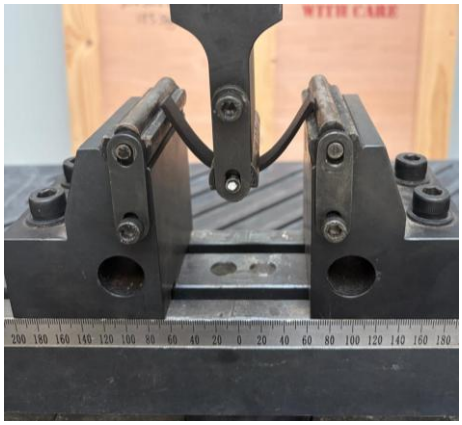


Figure 4.16: Carbon fibre-reinforced Onyx® flexural specimen during testing, showing displacement from the supports at large deformation.

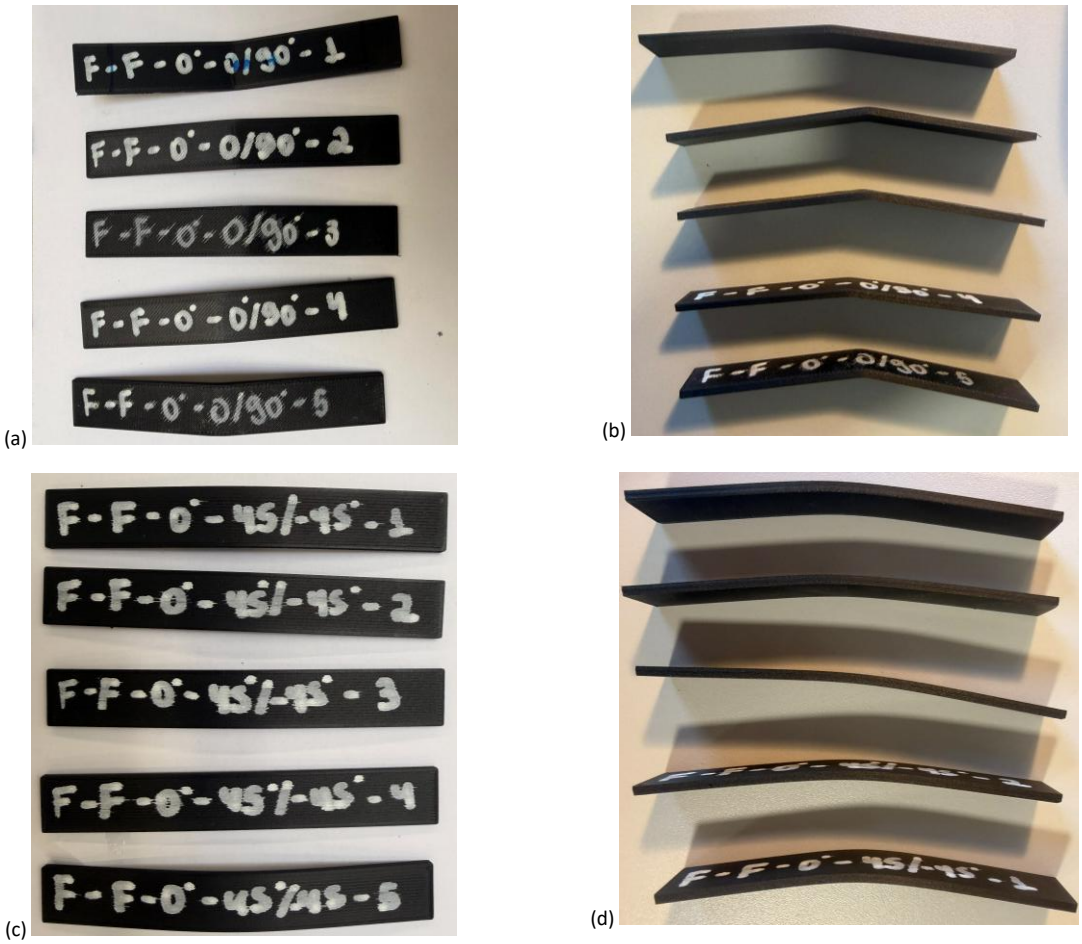
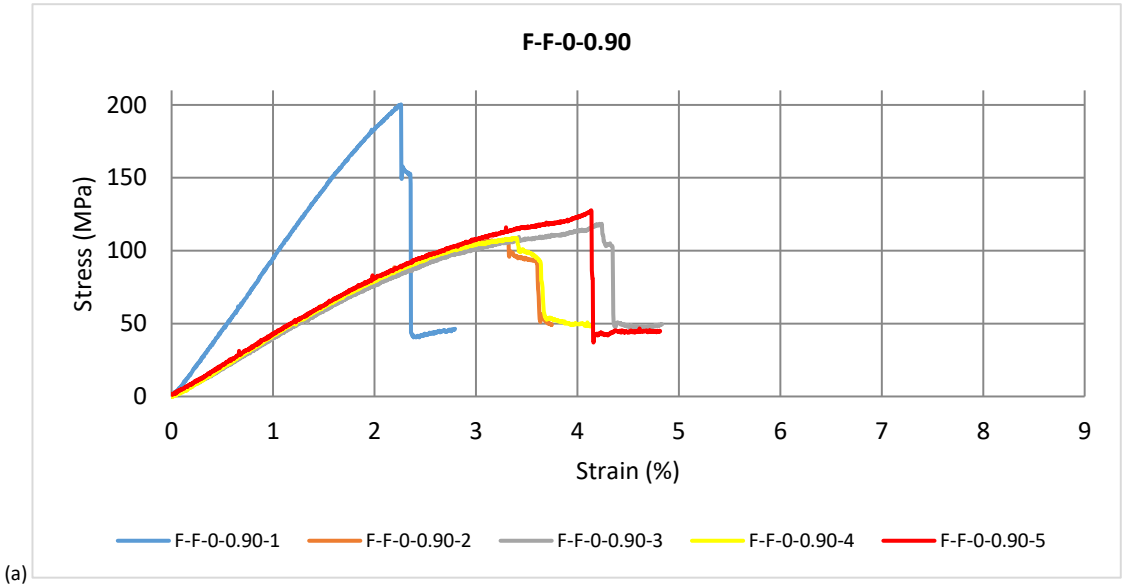
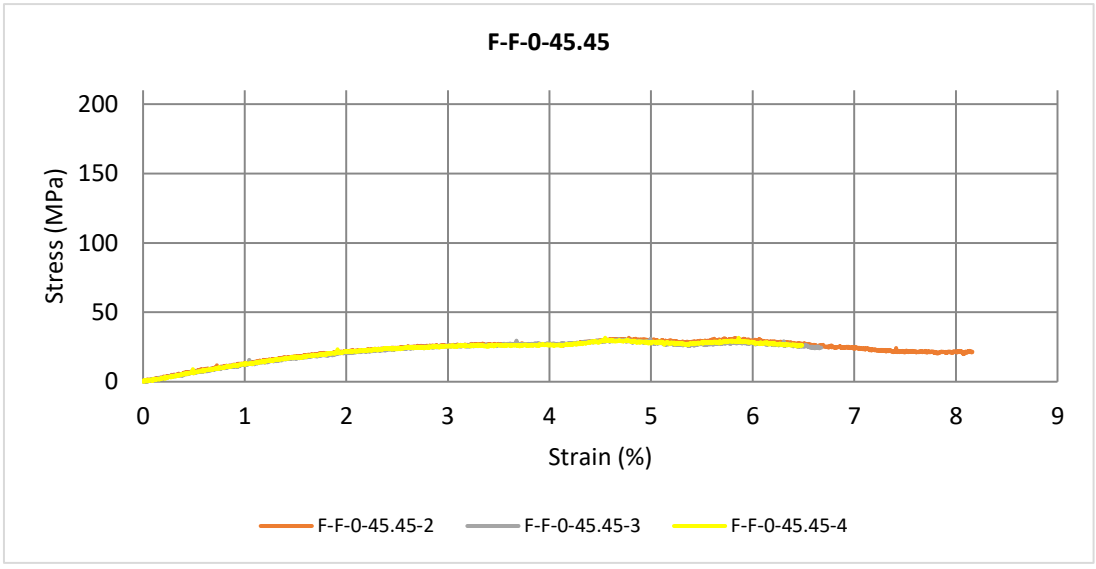


Figure 4.17: Carbon fibre-reinforced Onyx® flexural specimens after testing: (a) front view of specimens with 0°/90° printing bed orientation; (b) lateral view of the same specimens; (c) front view of specimens with 45°/−45° printing bed orientation; (d) lateral view of the same specimens.

The flexural stress–strain curves obtained for the two printing bed orientations are presented in **Figure 4.18**. The 0°/90° specimens showed an approximately linear response at the beginning of the test, followed by a progressive increase in stress until the maximum value was reached. The retained specimens from this configuration showed similar behaviour, although the stress level and strain at the selected maximum varied between specimens. In comparison, the 45°/−45° specimens showed a more consistent response, with the curves following a similar trend throughout the initial and intermediate stages of the test.



(a)



(b)

Figure 4.18: Engineering stress–strain curves obtained from the flexural tests of carbon fibre-reinforced Onyx® specimens: (a) 0°/90° printing bed orientation; (b) 45°/−45° printing bed orientation.

At higher deformation levels, the curves showed decreases and irregularities associated with the displacement of the specimens from the supports. The maximum flexural stress and corresponding strain were therefore determined from the stable portion of each curve, immediately before the onset of the irregular response. The flexural modulus was determined from the initial portion of the curve, before this behaviour occurred.

As discussed in Section 4.3 for the Onyx® specimens, the standard used here (BS EN ISO 14125:1998 + A1:2011) also assumes a constant support span, so the same caution regarding the calculated maximum flexural stress and strain applies below.

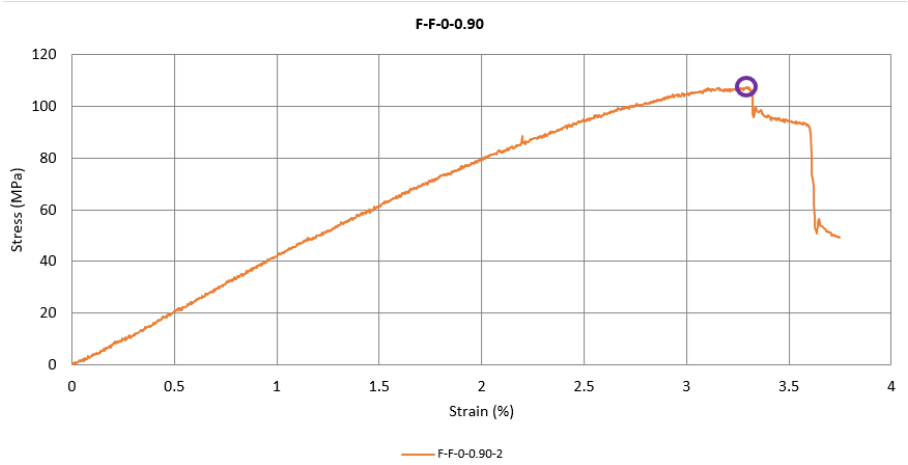


Figure 4.19: Example of the determination of the maximum flexural stress and corresponding strain from the stable portion of the stress–strain curve.

The 0°/90° specimens exhibited substantially higher flexural strength and stiffness than the 45°/−45° specimens. For the 0°/90° configuration, the average flexural strength was 115.61 ± 9.45 MPa, while the average flexural modulus was 3.83 ± 0.18 GPa. For the 45°/−45° configuration, the corresponding values were 31.39 ± 0.50 MPa and 1.20 ± 0.10 GPa, respectively. The average flexural strain was 4.38 ± 0.53% for the 0°/90° specimens and 4.77 ± 0.22% for the 45°/−45° specimens, indicating similar deformation levels at the selected maximum stress despite the substantial differences in strength and stiffness.

The statistical values were calculated excluding specimens that were not considered representative of the corresponding configuration. For the 0°/90° orientation, specimen 1 was excluded because it was manufactured with four floor layers instead of five. For the 45°/−45° orientation, specimens 1 and 5 were excluded due to technical problems during testing. The individual results and the corresponding statistical values are presented in **Table 4.4**.

Table 4.4: Flexural properties obtained for the carbon fibre-reinforced Onyx® specimens according to printing bed orientation.

F-F-0				
Printing bed Orientation	**Sample**	**Flexural strength (MPa)**	**Flexural Strain (%)**	**Flexural Modulus (GPa)**
0°/90°	1	200.35*	2.79*	8.57*
	2	107.59	3.75	4.08
	3	118.45	4.83	3.75
	4	108.65	4.14	3.67
	5	127.75	4.82	3.82
	Average	115.61	4.38	3.83
	Standard deviations	9.45	0.53	0.18
45°/-45°	1	**	**	**
	2	31.66	4.78	1.32
	3	30.81	4.99	1.14
	4	31.70	4.55	1.15
	5	**	**	**
	Average	31.39	4.77	1.20
	Standard deviations	0.50	0.22	0.10

Notes:
*Specimen was manufactured with four floor layers instead of five and was excluded from the calculation of the average and standard deviation.
** Specimens was excluded from the experimental results due to technical problems during testing.

A comparison with the Onyx® specimens tested under the same experimental programme shows that the measured effect of continuous carbon fibre reinforcement differed between the two printing bed orientations. For the 0°/90° configuration, the addition of continuous carbon fibre resulted in a substantial increase in both flexural strength and stiffness, with the average flexural strength increasing from 33.83 MPa for Onyx® to 115.61 MPa for the carbon fibre-reinforced specimens, while the flexural modulus increased from 1.54 GPa to 3.83 GPa. In contrast, the 45°/−45° carbon fibre-reinforced specimens exhibited lower average flexural strength and modulus than the corresponding Onyx® specimens, decreasing from 42.30 MPa to 31.39 MPa and from 1.96 GPa to 1.20 GPa, respectively.

The substantial difference observed between the two printing bed orientations, particularly in terms of flexural strength and modulus, was not fully expected, considering that the same material system and general manufacturing process were used. Several factors may

contribute to this difference, including variations in the amount or arrangement of continuous carbon fibre within the printed structure, the bonding between the carbon fibre and Onyx® matrix, or differences in the effective printing conditions. However, these factors were not independently investigated in the present study, and therefore no specific cause can be established from the available results.

4.5. Four-Point Bending Test of Sandwich Specimens

The manufactured sandwich specimens generally presented good printing quality. Some small imperfections in the surface finish were observed; however, no other significant manufacturing defects or differences between the specimens were identified. An example of the observed surface imperfections is presented in **Figure 4.20**.

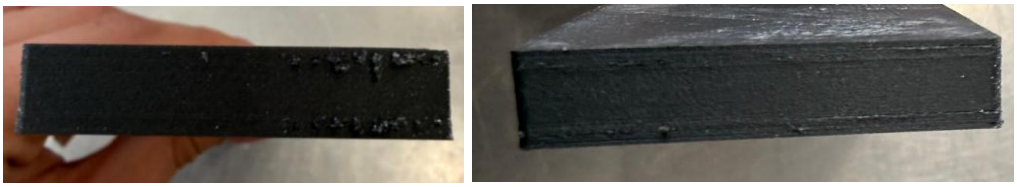


Figure 4.20: Surface imperfections observed on the manufactured sandwich specimens before testing.

The sandwich specimens before testing are presented in **Figure 4.21**. The three specimens presented similar overall geometry and surface condition.

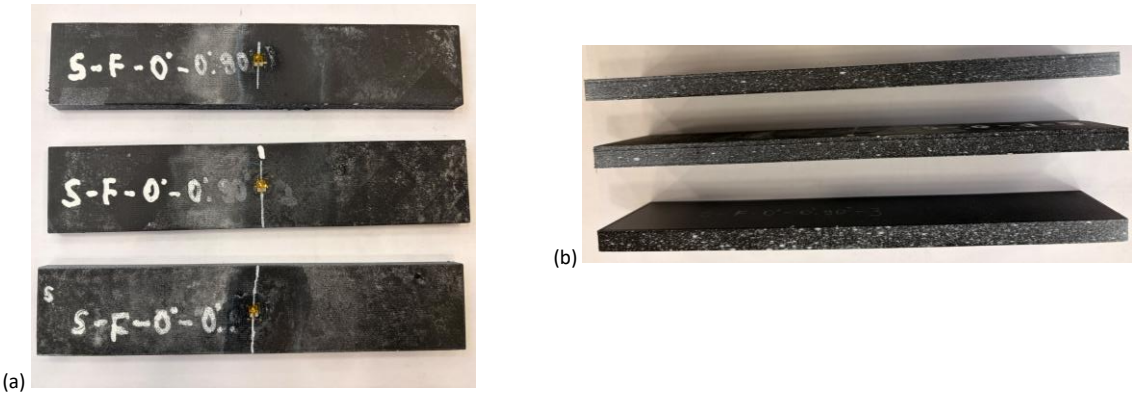


Figure 4.21: Sandwich specimens before the four-point bending tests: (a) top view; (b) lateral view.

During the four-point bending tests, the specimens underwent deformation while remaining largely intact. No complete fracture was observed during the tests. A representative specimen during testing is presented in **Figure 4.22**.

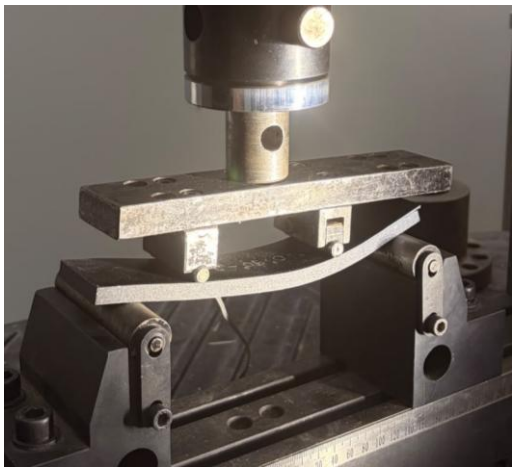
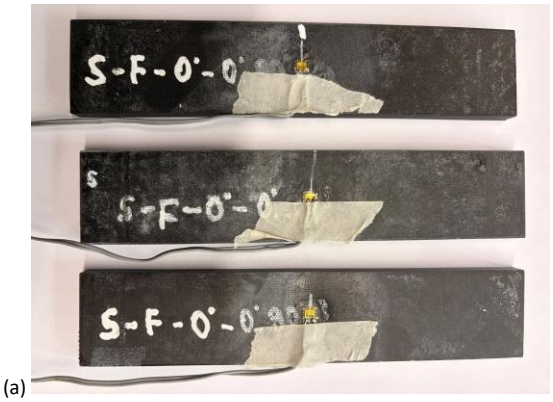


Figure 4.22: Sandwich specimen during the four-point bending test.

The post-test condition of the three sandwich specimens is presented in **Figure 4.23**. Local delamination between the facesheet and the core was observed in the some specimens.



(a)



(b)

Figure 4.23: Sandwich specimens after the four-point bending tests: (a) top view; (b) lateral view.

The load–displacement curves recorded during the four-point bending tests, corrected for the initial seating region, are presented in **Figure 4.24**. All three specimens exhibited an approximately linear initial response, followed by a first damage event identified by a sudden drop in the recorded load, after which the three specimens exhibited markedly different post-damage responses. Specimen 3 exhibited the most abrupt behaviour, with the load dropping by approximately 57% immediately after the first damage event. Specimen 1 retained a substantial residual load-carrying capacity after the initial drop, whereas Specimen 2 continued to gain load beyond its first damage point, subsequently reaching a global maximum load higher than the load recorded at first damage. This progressive, non-catastrophic response is consistent with localized internal damage rather than with complete failure of the specimens.

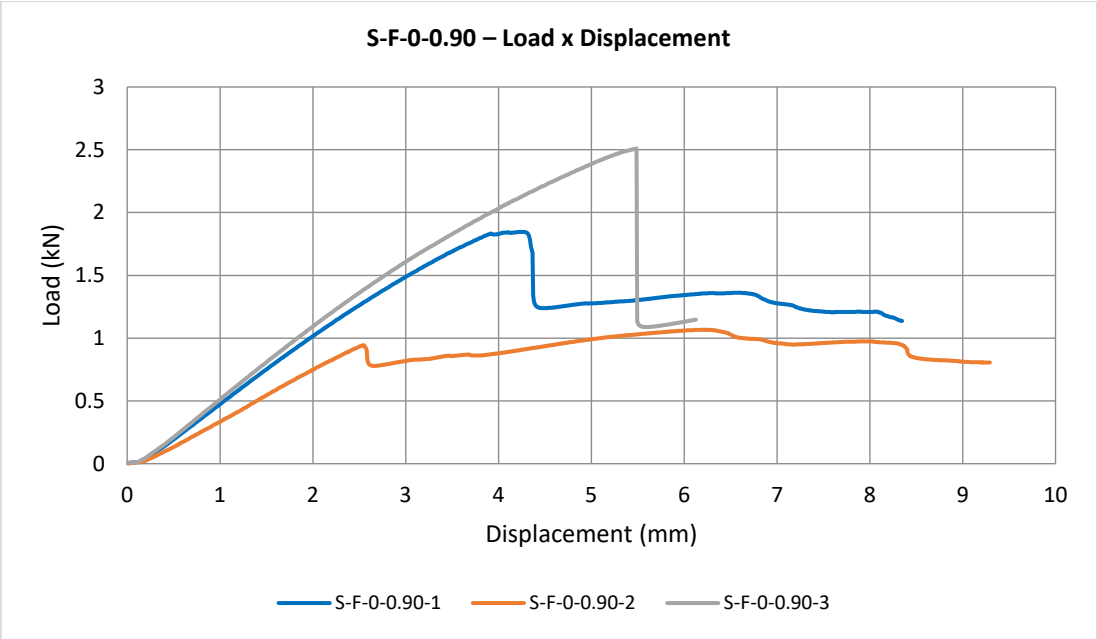


Figure 4.24: Load–displacement curves obtained from the four-point bending tests of the sandwich specimens, corrected for the initial seating region.

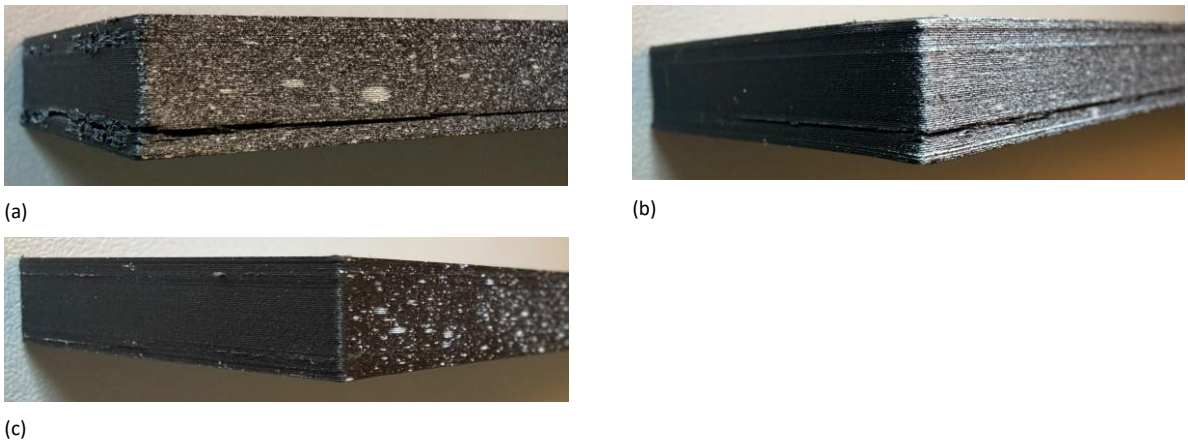


Figure 4.25: Close-up view of the post-test damage observed in each specimen: (a) S-F-0-0.90-1; (b) S-F-0-0.90-2; (c) S-F-0-0.90-3.

For each specimen, the initial stiffness was obtained from a linear regression of the corrected load–displacement curve between approximately 20% and 60% of the first damage load. The first damage event was identified as the first pronounced load drop observed in the curve. Where the maximum load did not coincide with the first damage event, both values were recorded separately. The resulting mechanical parameters are summarised in **Table 4.5**.

Table 4.5: Summary of the four-point bending test results obtained for the sandwich specimens from the crosshead displacement.

S-F-0-0.90						
Specimen	**k (kN/mm)**	**P_1 (kN)**	**δ_1 (mm)**	**Pmax (kN)**	**δmax (mm)**	**Total energy absorbed (J)**
1	0.541	1.847	4.121	1.847	4.121	9.649
2	0.413	0.944	2.368	1.067	6.041	7.440
3	0.558	2.510	5.429	2.510	5.429	8.339
Average	**0.504**	**1.767**	**3.973**	**1.808**	**5.197**	**8.476**
Standard deviation	**0.080**	**0.786**	**1.536**	**0.722**	**0.981**	**1.111**

Notes:
k = initial stiffness, from the crosshead displacement.P_1, δ_1 = load and displacement at the first damage event. Pmax, δmax = maximum load and corresponding displacement.

The initial stiffness of the three specimens was comparatively consistent, whereas the load and displacement associated with the first damage event were considerably more scattered. This is consistent with the different damage patterns observed after testing (**Figure 4.25**): Specimen 1 exhibited a delamination extending along a substantial portion of its length, Specimen 2 showed a smaller localized delamination across its width, and Specimen 3 showed no visible external damage despite reaching the highest load. Specimen 2 also exhibited a more gradual damage evolution, reaching its maximum load of 1.067 kN only after the first damage event at 0.944 kN. In contrast, for Specimens 1 and 3, the maximum load coincided with the first pronounced damage event.

The local bending strain was measured by the strain gauge bonded to the bottom face of each specimen, at mid-span, within the constant-moment region of the four-point bending configuration (section 3.7) The applied bending moment was obtained from the recorded load, M = Pa/2, where a = 40 mm is the support-to-load distance. The corresponding load–strain curves are presented in **Figure 4.26**.

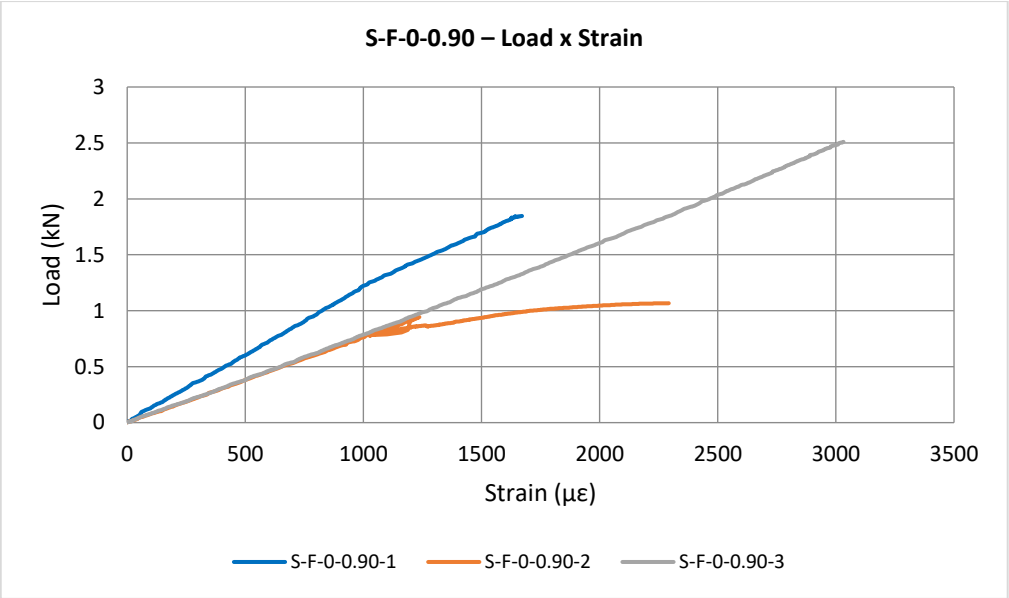


Figure 4.26: Load–strain curves obtained from the bottom mid-span strain gauge (SG1) during the four-point bending tests of the sandwich specimens (S-F-0-0.90).

Assuming the neutral axis to lie at mid-thickness, the bending rigidity of each specimen was estimated from the initial slope of the moment–curvature response, given by Equation (4.1). For comparison, an apparent bending rigidity was obtained from the crosshead displacement, using the standard elastic solution for a simply supported beam in four-point bending, Equation (4.2), with L = 160 mm the support span (section 3.7). The bending moment, strain and bending rigidity values obtained for the three specimens are summarised in **Table 4.6**.

$$EI_{\mathrm{SG}} = \frac{ah}{4}\frac{\mathrm{d}P}{\mathrm{d}\varepsilon} \tag{4.1}$$

$$EI_{\mathrm{cross}} = \frac{ka(3L^2 - 4a^2)}{48} \tag{4.2}$$

Table 4.6: Bending moment, strain and bending rigidity obtained for the sandwich specimens from the strain gauge (SG1) and from the crosshead displacement.

S-F-0-0.90						
Specimen	**ε_1 (με)**	**εmax (με)**	**M_1 (Nm)**	**Mmax (Nm)**	**SG1, $_{EISG}$ (Nm²)**	**EI_{cross} (Nm²)**
1	1671	1671	36.94	36.94	96.9	31.7
2	1237	2293	18.88	21.34	61.5	24.2
3	3032	3032	50.20	50.20	65.0	32.7
Average	**1980**	**2332**	**35.34**	**36.16**	**74.5**	**29.6**
Standard deviation	**937**	**681**	**15.72**	**14.45**	**19.5**	**4.7**

Notes:
ε_1, εmax = strain measured by SG1 at first damage and at maximum load.
M_1, Mmax = bending moment at first damage and at maximum load, from P_1 and Pmax using a = 40 mm.
EISG = bending rigidity from the strain gauge; EIcross = apparent bending rigidity from the crosshead displacement.

The bending rigidity estimated from the strain gauge measurements, EI_{SG}, was consistently higher than the apparent rigidity obtained from the crosshead displacement, EI_{cross}, for all three specimens. This difference was expected, since the crosshead displacement includes contributions beyond the bending deformation of the face sheets, namely the shear deformation of the core, local seating of the specimen at the loading and support rollers, and the compliance of the testing machine, whereas the strain gauge, bonded at mid-span within the constant-moment region, provides a more direct measurement of the local bending strain of the bottom face. Consequently, EI_{SG} is considered a more representative estimate of the flexural rigidity of the sandwich cross-section, while EI_{cross} should be interpreted as a global structural stiffness rather than as a section property. This gap between the two estimates is itself an indication that shear deformation of the core contributes appreciably to the overall deflection of the sandwich specimens under four-point bending.

The nominal sandwich geometry used for the calculations was defined in Eiger and is described in detail in section 3.1.2. The panel had a total nominal thickness of 8 mm and a width (b) of 39 mm. Treating each face sheet as a single effective layer and neglecting the bending contribution of the core, consistent with standard sandwich beam theory, the nominal face-sheet stress was obtained from Eq. (4.3), where d = 6.0625 mm is the distance between the face centroids, and t is the corresponding face thickness (2.125 mm top, 1.750 mm bottom). The resulting stresses are summarised in **Table 4.7**.

$$\sigma = \frac{M}{d \times b \times t} \tag{4.3}$$

Table 4.7: Nominal face-sheet stresses obtained for the sandwich specimens (S-F-0-0.90) using the sandwich force-couple approximation.

Specimen	Condition	M (Nm)	Compression face stress (MPa)	Tension face stress (MPa)
1	First damage = Max. load	36.94	-73.5	+89.3
2	First damage	18.88	-37.6	+45.6
2	Maximum load	21.34	-42.5	+51.6
3	First damage = Max. load	50.20	-99.9	+121.3

Notes:
M = bending moment (Table 4.6).
A negative stress denotes compression (top face); a positive stress denotes tension (bottom face).

The nominal face-sheet stresses obtained at the maximum load remained below the tensile strength reported for the carbon fibre-reinforced Onyx® (section 4.2), though above that of the plain Onyx® alone (section 4.1), which is consistent with the carbon-fibre layer carrying a disproportionate share of the load within the hybrid face sheet. Because each face sheet combines Onyx® with a stiffer carbon-fibre layer, this nominal value is an average over both materials, and the true stress within the carbon fibre itself may be higher.

The observed loss of load-carrying capacity is consistent with the delaminations observed in Specimens 1 and 2 (**Figure 4.25**); for Specimen 3, which showed no visible external damage despite the highest load and the most abrupt drop, the failure may instead have originated internally (for example, core crushing or fibre/matrix cracking beneath the surface), a mechanism that could not be confirmed from visual inspection alone and would benefit from closer microscopic examination in future work.

Because the initial elastic stiffness of the sandwich specimens was comparatively repeatable between specimens, the strain-gauge-based bending rigidity obtained in this section (**Table 4.6**) is expected to provide a suitable reference value for the validation of the linear-elastic response of the numerical model, whereas the prediction of the damage initiation load will likely require a more detailed representation of the face–core interface.

It should be noted that a speckle pattern was applied to the lateral surface of the specimens for digital image correlation (DIC), as described in Section 3.7. However, the images acquired during testing did not provide sufficient resolution for reliable correlation, and full-field strain data could therefore not be extracted.

5. NUMERICAL MODELLING

5.1. Finite Element Model

The numerical model was developed and analysed in Abaqus 2022 (Dassault Systèmes), using the Abaqus/Standard implicit solver.

The specimen geometry followed the layer arrangement shown in **Figure 3.3 (c)** and the nominal cross-section defined in **Table 3.1**. Each material layer (the two continuous carbon fibre-reinforced face sheets, the intermediate and external Onyx® layers and the triangular-infill core) was modelled as an individual solid part and stacked according to its nominal position.

In addition to the sandwich specimen itself, four rigid cylindrical rollers were added to the assembly to reproduce the four-point bending fixture: two support rollers and two loading rollers, spaced 160 mm and 80 mm apart, respectively, matching the spans defined for the experimental setup **Figure 3.12**.

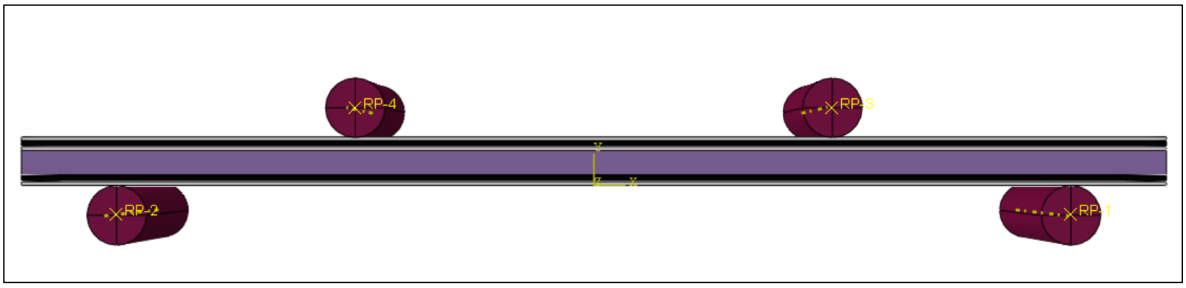


Figure 5.1: Finite element model assembly: sandwich specimen (face sheets, Onyx® layers and core) and the four rollers used to reproduce the four-point bending fixture.

Several works in the literature highlight the importance of accounting for the orthotropic behaviour of additively manufactured composite materials. In this work, however, the orthotropic elastic constants could not be obtained from the experimental characterisation performed in Chapter 4 without additional testing. An isotropic material description was therefore adopted as a simplification. Since the sandwich specimens were manufactured using the 0°/90° printing-bed orientation, the average tensile properties obtained for this

orientation in Chapter 4 were adopted as the equivalent isotropic Young's modulus for the Onyx® and carbon fibre-reinforced Onyx® materials. The core material was not characterised independently; its stiffness was estimated as half of the Onyx® tensile modulus, resulting in an equivalent homogenised modulus of 363 MPa. This approximation was adopted to represent the 50% triangular-infill core in the simplified numerical model. The resulting properties are summarised in **Table 5.1**.

Table 5.1: Isotropic elastic properties adopted for each material in the numerical model.

Material (model)	Property source	Young's modulus (MPa)	Poisson's ratio
Onyx®	Onyx® tensile test, 0°/90° (average)	726	0.35
Carbon fibre-reinforced Onyx®	Carbon fibre-reinforced Onyx® tensile test, 0°/90°, average	23 410	0.35
Core	50% of Onyx® tensile modulus	363	0.35

A Poisson's ratio of 0.35 was adopted for the three modelled materials. Similar values have been reported in the literature for Onyx® [25] [26]. The Poisson's ratios of the carbon fibre-reinforced Onyx® and the equivalent core material were not experimentally characterised in the present study and were also adopted as 0.35. Therefore, the use of the same value for all three materials represents a further simplification associated with the isotropic modelling approach.

In addition to the isotropic simplification, the material behaviour was modelled as purely linear elastic, with no plasticity or in-material damage criterion defined. Together with the fully bonded interfaces described below, this means that the model has no mechanism for representing permanent deformation or progressive material failure. The numerical results should therefore be interpreted primarily as representative of the linear, pre-failure response of the structure.

All layers were modelled using linear hexahedral solid elements with reduced integration (C3D8R) and assigned homogeneous solid sections corresponding to their respective materials, consistent with the isotropic, homogenised description adopted for the model.

A structured hexahedral mesh was used throughout. The same in-plane discretisation, comprising approximately 70 elements along the specimen length and 20 elements across its width, was applied to every layer, keeping the nodes aligned in-plane between adjacent layers. A uniform through-thickness element size of 0.125 mm, matching the nominal printed

layer height, was initially considered. However, the final mesh used an approximately uniform global element size across the assembly, resulting in different numbers of elements through each layer: one for the 0.125 mm Onyx® layer, two for the 0.5 and 0.625 mm Onyx® layers, three for the 1.000 mm carbon fibre-reinforced layers, and ten for the 4.125 mm core. This resulted in a coarser discretisation of the thinner layers and a finer discretisation of the core, while avoiding the substantially higher computational cost associated with applying a 0.125 mm element size throughout the model.

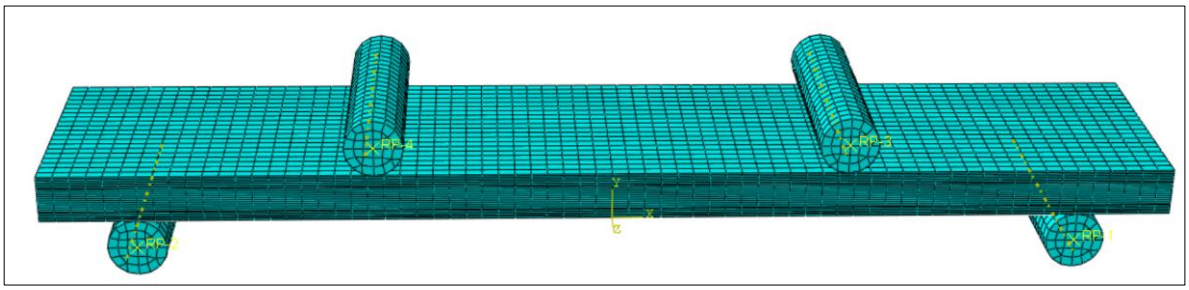


Figure 5.2: Mesh of the numerical model.

Each roller was modelled as a discrete rigid body and governed by a single reference point at its centreline, to which the corresponding boundary conditions were applied.

Contact was defined between each roller and its corresponding face sheet using surface-to-surface contact: the two support rollers were paired with the bottom face sheet, while the two loading rollers were paired with the top face sheet. A hard pressure-overclosure relationship was used in the normal direction, preventing surface interpenetration while allowing free separation. Coulomb friction was defined in the tangential direction using a friction coefficient of 0.2. All internal interfaces between adjacent material layers were modelled as fully tied constraints.

The two support rollers were fully fixed in all degrees of freedom. The two loading rollers were constrained to move only in the vertical direction and were driven simultaneously by a prescribed downward displacement of up to 6 mm.

The analysis was performed using a single Static General step with the nonlinear geometry option activated to account for the geometric changes associated with bending. Automatic stabilisation was employed to assist convergence during the contact-dominated analysis. The stabilisation parameters were defined using stabilize = 0.0002 and ALLSDTOL = 0.05, allowing the stabilisation damping to be adjusted automatically during the analysis while limiting the

stabilisation energy relative to the strain energy. Automatic incrementation was adopted, with an initial increment of 0.001, a maximum increment of 1.0 and a minimum increment of 10^{-20}.

5.2. Numerical Results

The analysis was carried through to full completion, reaching the target displacement of 6 mm over 228 increments. A small number of increments required automatic cutbacks before converging, as expected for a contact-dominated analysis. The resulting force-displacement response is shown in **Figure 5.3**. The total reaction force from the two loading rollers increased with displacement throughout the analysis, reaching approximately 2.07 kN at the prescribed displacement of 6 mm.

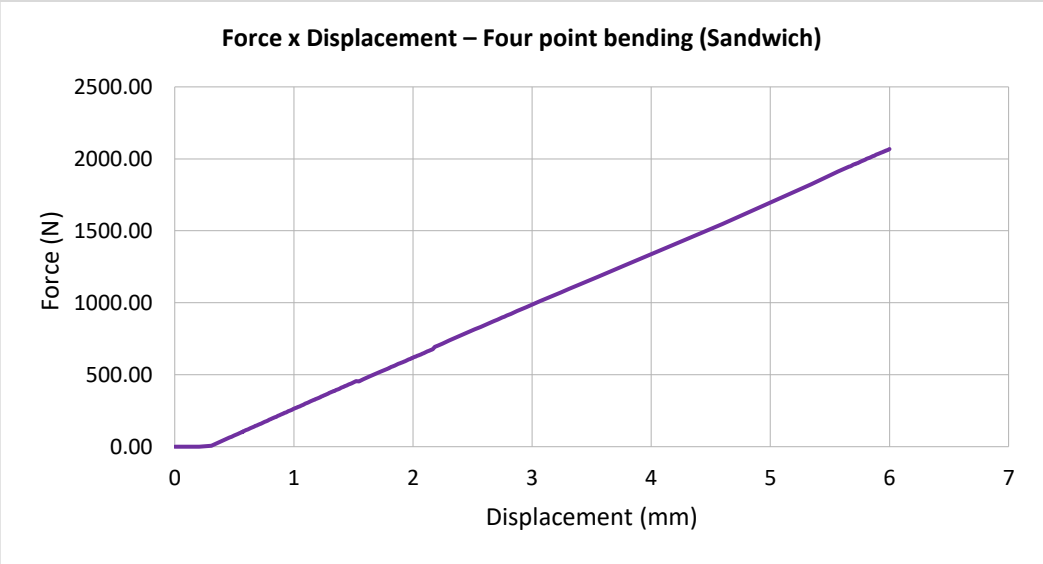


Figure 5.3: Force-displacement curve obtained from the numerical model, combining the reaction forces at the two loading rollers.

Several checks were performed to assess the numerical stability and physical consistency of the model. The ratio between the artificial energy introduced by the automatic stabilisation scheme (ALLSD) and the internal strain energy of the model (ALLIE) was monitored throughout the analysis. Excluding the initial increments of the step, during which the internal energy had not yet sufficiently developed, this ratio remained below 0.29% for the remainder of the analysis. This value is substantially below the 5% stabilisation-energy tolerance specified for

the analysis step, indicating that the contribution of artificial stabilisation energy was negligible and did not significantly influence the numerical response.

The reaction forces at the two loading rollers (−1034.24 N and −1033.91 N) and at the two support rollers (1033.81 N and 1033.65 N) differed by less than 0.03% within each pair, indicating a symmetric response consistent with the specimen and fixture geometry. The total support reaction (2067.46 N) differed from the total loading reaction (2068.15 N) by approximately 0.03%, confirming that the model remained in close static equilibrium throughout the analysis.

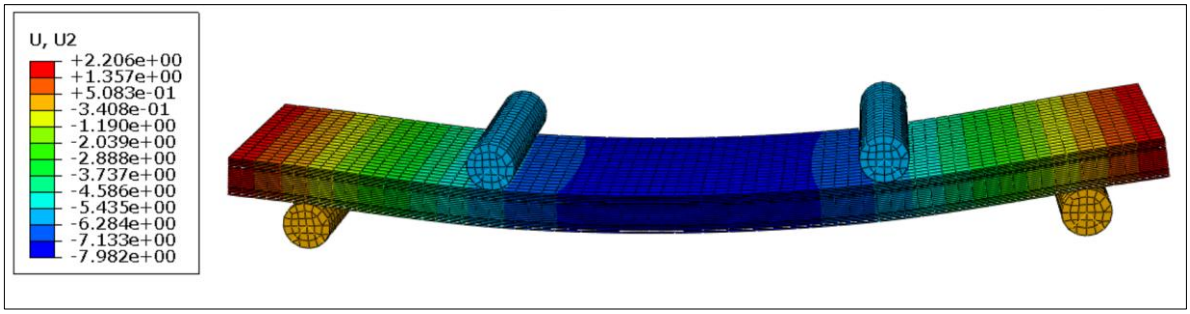


Figure 5.4: Deformed shape of the model (U2 displacement contour) at the final increment, corresponding to a prescribed displacement of 6 mm.

5.3. Comparison of Numerical with Experimental Results

The numerical stiffness was obtained from a linear regression on the elastic region of the curve (displacement between −1 and −5 mm), excluding the initial roller-specimen gap closure. Since the model is purely elastic and has fully bonded interfaces, it does not exhibit a distinct failure point. Therefore, the numerical force was evaluated by interpolation at the experimental maximum displacement to allow comparison with the experimental response. The results are compared with the experimental values from **Table 4.5** in **Table 5.2**.

Table 5.2: Comparison between the numerical model and the experimental results from Table 4.5.

Parameter	FEA	Table 4.5 (experimental)	Difference
Stiffness (kN/mm)	0.359	0.504	−28.8%
Maximum Load at Maximum Displacement (kN)	1.770	1.808	−2.1%
Maximum Displacement (mm)	5.197 (evaluation point)	5.197	—

The comparison shows a clear difference between the two metrics: the numerical stiffness is under-predicted by 28.8%, while the force evaluated at the Maximum Displacement experimental is under-predicted by only 2.1%. The difference in stiffness can be attributed to the simplifications adopted in the numerical model, particularly the representation of the core. The core stiffness was estimated as half of the Onyx® tensile modulus and therefore does not capture the actual behaviour of the 50% triangular-infill core, including its likely anisotropic and shear response. Since the core contributes significantly to the shear deformation of a sandwich structure, this simplification is considered a plausible contributor to the stiffness difference. Other modelling assumptions, including the isotropic material representation and fully bonded interfaces, may also contribute to the difference.

The closer agreement in the force at the Maximum Displacement indicates that, at this evaluation point, the simplified model is able to reproduce the experimental load with a difference of only approximately 2%. This may indicate a greater influence of the face sheets on the load carried by the structure at larger displacements, as their elastic properties were obtained directly from the experimental tensile characterisation. However, the contribution of the different modelling assumptions cannot be isolated from the present analysis.

Figure 5.5 compares the numerical force-displacement curve with the three individual experimental curves. The experimental curves show load drops between approximately 4 and 6 mm of displacement, associated with the delamination reported in Section 4.5. Since the numerical model has no damage or interfacial-separation criterion, it does not reproduce these load drops and instead continues to increase smoothly, as expected. Up to and around the experimental Maximum Displacement, the numerical curve remains within the range of the experimental responses and passes close to the experimental average point, consistent with the 2.1% difference in force reported above.

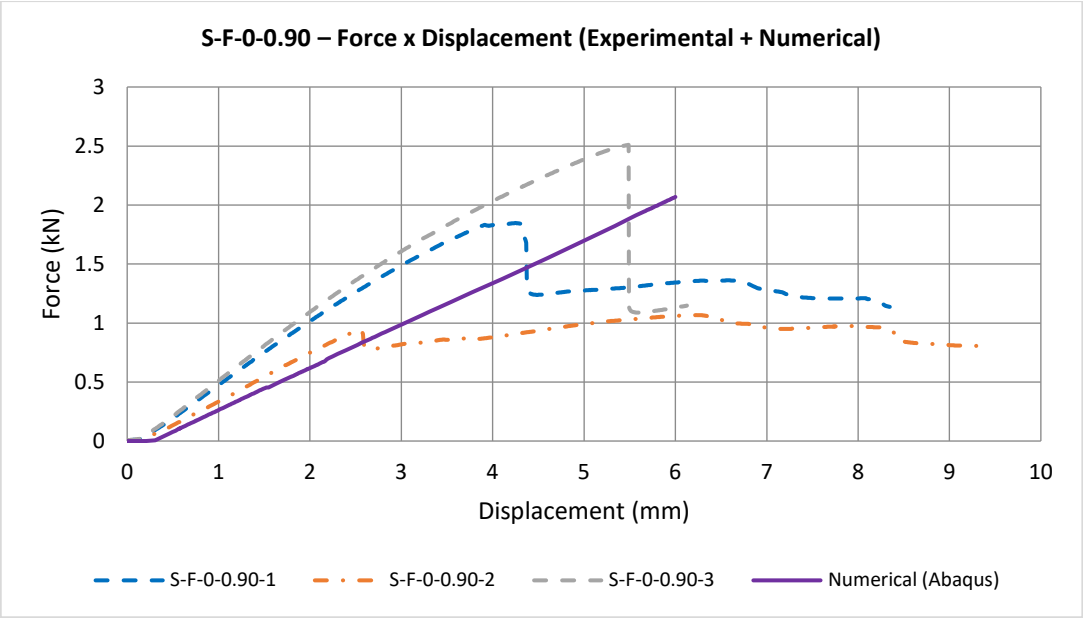


Figure 5.5: Comparison between the numerical force-displacement curve and the experimental curves of the three S-F-0-0.90 specimens.

The comparison also highlights the specimen-to-specimen variability in the manufactured samples, with peak loads ranging from 1.07 to 2.51 kN across the three tests. This variability should be considered when interpreting the numerical-experimental comparison, particularly since the experimental reference values are based on only three specimens. Overall, the numerical model provides a reasonable representation of the global force-displacement response up to the experimental displacement level, while the differences in stiffness and the absence of the experimental failure behaviour reflect the simplifications adopted in the model.

6. CONCLUSIONS AND FURTHER DEVELOPMENTS

6.1. Main conclusions

The main objective of this thesis was to investigate the mechanical and structural behaviour of additively manufactured sandwich structures composed of an Onyx® core and continuous carbon fibre-reinforced face sheets manufactured using the Markforged Mark Two system. The study combined experimental characterisation of the printed materials, evaluation of the flexural behaviour of the sandwich structure and finite element modelling.

The experimental programme was constrained by practical limitations, including limited material availability and restrictions imposed by the proprietary Markforged Eiger system, which limited the control and characterisation of some manufacturing parameters. Manufacturing imperfections and the resulting specimen-to-specimen variability also affected the extent of the experimental programme and should therefore be considered when interpreting the results. Overall, the findings demonstrate that the mechanical response was governed not only by the printing configuration and the presence of continuous fibre reinforcement, but also by manufacturing consistency.

For the printed Onyx® specimens, the tensile tests showed that the printing bed orientation had a limited influence on tensile strength, with average values of 27.47 ± 4.24 MPa for the 0°/90° configuration and 26.40 ± 3.64 MPa for the 45°/−45° configuration. A more pronounced effect was observed in stiffness and deformation capacity: the 45°/−45° configuration presented a higher tensile modulus (1.19 ± 0.30 GPa versus 0.73 ± 0.11 GPa), while the 0°/90° configuration exhibited substantially greater strain at failure (36.32 ± 1.00% versus 19.37 ± 0.60%). Thus, the printing bed orientation had little effect on tensile strength but significantly influenced the stiffness and deformation behaviour of the printed Onyx®.

The carbon fibre-reinforced Onyx® specimens showed a strong dependence on manufacturing quality. Specimens 3–5, which presented comparatively better manufacturing quality, reached an average tensile strength of 347.42 ± 61.13 MPa, tensile modulus of 23.41 ± 2.33 GPa and tensile strain of 1.41 ± 0.12%, whereas specimens 6–8, which presented more pronounced manufacturing imperfections, reached 124.30 ± 39.91 MPa, 11.09 ± 1.96 GPa and

1.10 ± 0.13%, respectively. The different responses and absence of a complete visible fracture in specimens 6–8 highlight the importance of manufacturing consistency, although a direct causal relationship cannot be established from the available results. For the 0°/90° configuration, the better-quality carbon fibre-reinforced specimens exhibited approximately 12.6 times higher tensile strength and 32 times higher tensile modulus than the unreinforced Onyx® specimens, while showing substantially lower tensile strain. This demonstrates the strong effect of continuous carbon fibre reinforcement on tensile strength and stiffness.

In flexure, both Onyx® and carbon fibre-reinforced Onyx® specimens exhibited substantial deformation without complete visible fracture. At high deformation levels, support displacement affected the later portion of the recorded response; therefore, the flexural properties were determined from the stable portion of the curves, while the flexural modulus was obtained from the initial linear response.

For the Onyx® specimens, the 45°/−45° configuration exhibited higher flexural strength and stiffness than the 0°/90° configuration. The average flexural strength increased from 33.83 MPa to 42.30 MPa, while the flexural modulus increased from 1.54 GPa to 1.96 GPa, corresponding to increases of approximately 25% and 27%, respectively. In contrast, the average flexural strain at the selected maximum stress decreased from 6.60% to 5.84%. These results indicate that the printing bed orientation influenced both the strength and stiffness of the Onyx® specimens under flexural loading, with the 45°/−45° configuration providing a stronger and stiffer response but lower strain at the selected maximum stress.

The flexural response of the carbon fibre-reinforced Onyx® specimens was strongly dependent on the printing bed orientation. The 0°/90° configuration presented an average flexural strength of 115.61 ± 9.45 MPa and flexural modulus of 3.83 ± 0.18 GPa, compared with 31.39 ± 0.50 MPa and 1.20 ± 0.10 GPa, respectively, for the 45°/−45° configuration. The corresponding average flexural strains were 4.38 ± 0.53% and 4.77 ± 0.22%, indicating similar deformation levels despite the substantial differences in strength and stiffness.

Compared with Onyx® under the same orientations, reinforcement increased flexural strength and modulus by approximately 242% and 149%, respectively, for 0°/90°, but reduced them by approximately 26% and 39%, respectively, for 45°/−45°. This unexpected orientation-dependent response needs further investigation.

The structural response of the sandwich specimens under four-point bending was evaluated for the S-F-0-0.90 configuration. The initial elastic stiffness was comparatively consistent between specimens (k = 0.504 ± 0.080 kN/mm), whereas the load and displacement associated with the first damage event were considerably more scattered (P_1 = 1.767 ± 0.786 kN). Post-test inspection showed that the specimens failed through different mechanisms: Specimen 1 developed a delamination extending along a substantial portion of its length, Specimen 2 showed only a small, localized delamination across its width, and Specimen 3, despite reaching the highest load, showed no visible external damage. This indicates that, while the elastic response of the sandwich structure was repeatable, the onset of damage was highly sensitive to local, specimen-specific factors.

The bending rigidity estimated from the strain gauge measurements (EISG = 74.5 ± 19.5 Nm²) was consistently higher than the apparent rigidity obtained from the crosshead displacement (EIcross = 29.6 ± 4.7 Nm²), confirming that shear deformation of the core, together with seating and machine compliance, contributed appreciably to the measured global displacement. Because only a single support span was tested, these two contributions could not be separated experimentally, and this is identified as a recommendation for future testing of these panels.

The nominal stresses obtained in the face sheets at maximum load remained below the tensile strength of the carbon fibre-reinforced Onyx® characterised in section 4.2, though above that of the plain Onyx® alone, consistent with the carbon-fibre layer carrying a disproportionate share of the load within the hybrid face sheet.

The delaminations observed in Specimens 1 and 2 point to the face–core interface as an important factor in the structural response, whereas the absence of visible damage in Specimen 3 suggests that its failure may have originated internally and could not be fully characterised from visual inspection. The strain-gauge-based bending rigidity is expected to provide a suitable reference for validating the linear-elastic response of the numerical model, while predicting the damage initiation load will likely require a more detailed representation of the face–core interface.

A finite element model was developed to reproduce the four-point bending response of the S-F-0-0.90 sandwich configuration. The model provided a reasonable representation of the global response, with a numerical stiffness of 0.359 kN/mm compared with 0.504 kN/mm

experimentally, while the force at the experimental maximum displacement differed by only 2.1% (1.770 kN versus 1.808 kN). The difference in stiffness was attributed mainly to the simplifications adopted in the numerical model, particularly the equivalent representation of the 50% triangular-infill core. The fully bonded interfaces and linear elastic material formulation also prevented the model from reproducing the face-core delamination observed experimentally. Overall, the model provided a useful numerical baseline for the elastic response of the sandwich structure and can be further refined through improved core characterisation and the inclusion of damage or interfacial separation.

Overall, these results confirm that the mechanical response of this Onyx® and continuous carbon fibre sandwich system is shaped by the combined effect of printing configuration, reinforcement and manufacturing consistency, and show that a linear-elastic finite element model, despite its simplifications, can already capture the sandwich structure's overall response reasonably well. Together, the experimental and numerical work developed in this thesis provides an initial characterisation of this specific AM sandwich configuration and a starting point for the developments discussed in the following section.

6.2. Further developments

The experimental and numerical work developed in this thesis provides a first characterisation of this specific Onyx® and continuous carbon fibre sandwich system, and several aspects that could not be fully addressed within the available time and resources remain open for future work. These follow naturally from the three levels considered throughout the thesis: the printed materials, the structural behaviour of the sandwich panel, and the finite element model built to represent it.

Only a small number of printing bed orientations were compared for each material and test type, so a more systematic investigation of the remaining printing parameters, namely raster angle, fibre orientation, infill density and layer configuration, would help separate their individual effects on the mechanical response. Increasing the number of specimens in the configurations most affected by material availability or technical problems during testing would also improve the statistical confidence of the reported properties, and repeating the flexural tests under the manufacturer's own testing standard, ASTM D7901, would allow a

more direct comparison with the properties reported by Markforged. Because none of the Onyx® or carbon fibre-reinforced Onyx® specimens fractured completely, the flexural properties had to be extracted from the stable portion of the curve before the specimens moved off the supports; accounting for the actual, changing span length as the specimen deflects, rather than discarding this later part of the response, would make better use of the recorded data.

A genuine orthotropic characterisation of the printed materials is also still missing. The two build orientations tested in this work each produce a fixed pair of raster angles, either 45°/−45° or 0°/90°, since the Eiger software always alternates the matrix raster in this way; isolating the properties along a single fibre or raster direction would require a different specimen design or build strategy. For the carbon fibre-reinforced material, this is not simply a matter of printing more samples, since the standard-sized tensile specimen for the 45°/−45° configuration exceeded the build volume of the Mark Two printer and could not be manufactured at all. Closing this gap would also help explain one of the more unexpected results of this thesis: the same continuous carbon fibre reinforcement increased the flexural strength and stiffness substantially in the 0°/90° configuration but reduced them in the 45°/−45° configuration, relative to the unreinforced Onyx®.

Because the response of the printed composite depends on how much continuous fibre is used and how the reinforcing layers are arranged within the stack, and not only on the properties of the fibre itself, varying the fibre content and the position of the carbon fibre layers is a related direction worth pursuing. The manufacturing imperfections observed in the specimens produced as the carbon fibre spool neared depletion are a separate open question, since a link between the remaining material supply and the reduced tensile performance of those specimens was observed but never confirmed.

The core of the sandwich was never characterised on its own; its stiffness was only estimated as half of the Onyx® tensile modulus for use in the numerical model. Dedicated tests on the core alone, namely a flexural test together with the shear, compression and flatwise tensile tests commonly used for sandwich cores in the literature, would replace this assumption with a measured property, and testing different infill patterns and densities would show how sensitive the structural response is to the specific 50% triangular configuration used in this work.

At the structural level, only a single support span was tested in the four-point bending tests, so the bending and shear contributions to the measured stiffness could not be separated; testing the same panel configuration over at least one additional span, following standard sandwich-beam practice, remains the clearest way to resolve this. While the initial stiffness of the three tested specimens was repeatable, the load at which the first damage occurred was not, ranging from under 1 kN to over 2.5 kN, so more specimens are needed specifically to characterise this scatter with any confidence. Given the orientation-dependent reversal noted above for the flat material specimens, it would also be worth manufacturing and testing a sandwich configuration with the 45°/−45° orientation, since the only configuration tested in this thesis was 0°/90°, and it is not yet known whether the same reversal carries through to the full structural response.

A few complementary diagnostic techniques would also help interpret these structural tests. Specimen 3 is a particularly interesting case, since it reached the highest load and failed most abruptly of the three, yet showed no visible external damage; microscopy or computed tomography (CT) scanning of the tested specimens would help determine whether its failure originated inside the core or at a hidden interface and could be applied to the other specimens for comparison. The speckle pattern applied for DIC did not lead to usable results, since the acquired images lacked sufficient resolution for reliable correlation; a revised camera setup and pattern would be needed to obtain the full-field strain data this technique was intended to provide, which otherwise remained limited to a single strain gauge reading in this work. A related limitation is that the carbon fibre-reinforced Onyx® modulus used throughout the thesis comes from coupons that combine Onyx® and carbon fibre together, so the face sheets could only be treated as a single homogenised layer when estimating their stresses; a specimen that isolates the continuous fibre layer on its own would allow a proper layer-by-layer stress analysis in future work.

These experimental refinements would feed directly into an improved numerical model. The most immediate change would be to replace the isotropic material description with orthotropic properties once these become available, since the printing process is known to introduce direction-dependent behaviour. Introducing plasticity and damage into the material model, together with a cohesive or otherwise damageable representation of the face-core interface in place of the fully tied constraint used here, would also allow the model to capture

the non-catastrophic load drops observed experimentally in two of the three specimens, rather than only the initial linear response.

The through-thickness mesh used in the reported model mixed different element counts across layers to limit computational cost; a fully uniform 0.125 mm mesh, matching the actual printed layer height, was considered during the development of the model but not carried through to the final analysis, and remains worth checking for its influence on the results. The core, identified as the main source of the roughly 29% under-prediction of the experimental stiffness, would benefit most from the properties measured in the tests proposed above, or even from its true internal geometry, which could be reconstructed by sectioning a manufactured specimen and imaging the exposed infill with the same microscopy or CT techniques suggested earlier, and used directly to build a geometrically accurate mesh in place of the homogenised approximation adopted in this work.

Bringing these refinements together and re-validating the resulting model against an expanded experimental dataset would be the natural continuation of this work, moving it from the elastic baseline established here towards a genuinely predictive tool for the design of this class of 3D-printed sandwich structures.

REFERENCES

[1] T. Zhao, J. Yang, J. Chen, and S. Guan, 'Review of carbon fiber-reinforced sandwich structures', *Polymers and Polymer Composites*, vol. 30, p. 09673911221098729, Jan. 2022, doi: 10.1177/09673911221098729.

[2] B. Castanie, C. Bouvet, and M. Ginot, 'Review of composite sandwich structure in aeronautic applications', *Composites Part C: Open Access*, vol. 1, p. 100004, Aug. 2020, doi: 10.1016/j.jcomc.2020.100004.

[3] J. Bühring, J. Zimmermann, M. Z. Sadeghi, A. Akhavan-Safar, L. F. M. Da Silva, and K.-U. Schröder, 'Experimental and numerical investigation of adhesively bonded additive manufactured sandwich structures with a pyramidal lattice core', *The Journal of Adhesion*, vol. 100, no. 5, pp. 323–339, Apr. 2024, doi: 10.1080/00218464.2021.1907571.

[4] N. S. Fatima, G. S. Dhaliwal, and G. Newaz, 'Influence of interfacial adhesive on impact and post-impact behaviors of CFRP/end-grain balsawood sandwich composites', *Composites Part B: Engineering*, vol. 212, p. 108718, May 2021, doi: 10.1016/j.compositesb.2021.108718.

[5] K. Nishi, Y. Sato, and J. Yanagimoto, 'Integral forming of continuous CFRP sandwich sheet by additive manufacturing', *Int J Mater Form*, vol. 16, no. 6, p. 63, Nov. 2023, doi: 10.1007/s12289-023-01788-7.

[6] O. Can Zehni, J. Xu, T. Lowe, E. Whitehouse, and A. Ataş, 'Continuous carbon fibre reinforced 3D-printed composites: impact damage and compression after impact (CAI) performance', *Composites Part A: Applied Science and Manufacturing*, vol. 198, p. 109097, Nov. 2025, doi: 10.1016/j.compositesa.2025.109097.

[7] C. Burnett, G. Graninger, Z. Eren, B. G. Falzon, and Z. Kazanci, 'Tensile Performance of Carbon Fibre-Reinforced 3d-Printed Polymers: Effect of Printing Parameters', 2025, *SSRN*. doi: 10.2139/ssrn.5149615.

[8] C. Huang, M. Norton, and M. W. Joosten, 'Investigating the mode one interlaminar performance of semi-woven 3D printed hybrid composites', *Composite Structures*, vol. 354, p. 118802, Jan. 2025, doi: 10.1016/j.compstruct.2024.118802.

[9] B. A. Kumar, K. S. Kumar, and A. C. Reddy, 'Mechanical properties of 3D-printed Onyx-fibreglass composites: Role of roof layers on tensile strength and hardness – Using anova technique', *Next Materials*, vol. 8, p. 100650, Jul. 2025, doi: 10.1016/j.nxmate.2025.100650.

[10] J. G.-M. Caraballo, S. Corbera, D. G. Gómez, and R. Barea, '1 An automated workflow to optimize 3D printed 2 continuous carbon fiber composite parts'.

[11] V. Kaushik, S. Kurra, and R. Adusumalli, 'Structure–property relationships in 3D-printed onyx-based composites reinforced with continuous fibers: role of temperature and fiber orientation', *Composites Part C: Open Access*, vol. 18, p. 100649, Oct. 2025, doi: 10.1016/j.jcomc.2025.100649.

[12] E. Polyzos, I. A. Rodrigues Lopes, P. P. Camanho, D. Van Hemelrijck, and L. Pyl, 'Continuum damage modeling of unidirectional 3D-printed composites under longitudinal tension', *Composites Part A: Applied Science and Manufacturing*, vol. 193, p. 108850, Jun. 2025, doi: 10.1016/j.compositesa.2025.108850.

[13] K. Mizukami and K. Nakamura, ‘Dual-nozzle 3D printing of fiber composites for fabrication of compliant lever-type vibration isolators with wide stopband’, *Thin-Walled Structures*, vol. 208, p. 112799, Mar. 2025, doi: 10.1016/j.tws.2024.112799.
[14] T. Ho-Nguyen-Tan, Y. J. Kim, G. S. Shin, J. Y. Hwang, M. Kim, and S. H. Yoon, ‘Anisotropic topology optimization and 3D printing for composite structures with tailored continuous carbon fiber paths’, *Composites Part B: Engineering*, vol. 299, p. 112371, Jun. 2025, doi: 10.1016/j.compositesb.2025.112371.
[15] X. S. Liew, ‘Stiffness analysis of a nylon sandwich core structure produced by a Markforged Mark Two printer’.
[16] N. Maqsood, M. Rimašauskas, M. Ghobakhloo, G. Mordas, and K. Skotnicová, ‘Additive manufacturing of continuous carbon fiber reinforced polymer composites using materials extrusion process. Mechanical properties, process parameters, fracture analysis, challenges, and future prospect. A review’, *Adv Compos Hybrid Mater*, vol. 7, no. 6, p. 202, Dec. 2024, doi: 10.1007/s42114-024-01035-w.
[17] ‘Industrial Additive Manufacturing Platform | Markforged’. Accessed: Jun. 16, 2026. [Online]. Available: https://markforged.com/
[18] C. Dong, ‘Finite Element Analysis of Additively Manufactured Continuous Carbon Fiber-Reinforced Composites’, *JOM*, vol. 75, no. 10, pp. 4150–4157, Oct. 2023, doi: 10.1007/s11837-023-06041-9.
[19] Markforged, ‘Composite material Datasheet’. Oct. 10, 2023. Accessed: Aug. 13, 2026. [Online]. Available: https://markforged.com/materials/plastics/onyx
[20] M. Kubota, K. Hayakawa, and A. Todoroki, ‘Effect of build-up orientations and process parameters on the tensile strength of 3D printed short carbon fiber/PA-6 composites’, *Advanced Composite Materials*, vol. 31, no. 2, pp. 119–136, Mar. 2022, doi: 10.1080/09243046.2021.1930497.
[21] A. Kumar and A. Kumar, ‘Influence of Raster Angle and Infill Pattern on the Mechanical Performance of Additively Manufactured Carbon Fiber Composite’, *Def. Sc. J.*, vol. 75, no. 5, pp. 629–636, Sep. 2025, doi: 10.14429/dsj.20343.
[22] S. Sangaletti, M. T. Aranda, L. Távara, and I. G. García, ‘Effect of stacking direction and raster angle on the fracture properties of Onyx 3D printed components: A mesoscale analysis’, *Theoretical and Applied Fracture Mechanics*, vol. 129, p. 104228, Feb. 2024, doi: 10.1016/j.tafmec.2023.104228.
[23] Wolf, T., ‘Vorschläge für mechanische Validierungsversuche an mit einem Markforged Mark Two Drucker hergestellten Sandwichproben’, Hochschule für Angewandte Wissenschaften Hamburg, Hamburg, Projektarbeit, 2020.
[24] A. Batley, R. Glithro, B. Dyer, and P. Sewell, ‘Evaluation of Tensile Strength and Repeatability of 3D Printed Carbon Fiber Materials and Processes’, *3D Printing and Additive Manufacturing*, vol. 11, no. 5, pp. 1691–1702, Oct. 2024, doi: 10.1089/3dp.2022.0262.
[25] G.-W. Lee, T.-H. Kim, J.-H. Yun, N.-J. Kim, K.-H. Ahn, and M.-S. Kang, ‘Strength of Onyx-based composite 3D printing materials according to fiber reinforcement’, *Front. Mater.*, vol. 10, p. 1183816, Apr. 2023, doi: 10.3389/fmats.2023.1183816.
[26] Z. Eren, C. A. Burnett, D. Wright, and Z. Kazancı, ‘Compressive characterisation of 3D printed composite materials using continuous fibre fabrication’, *International Journal of Lightweight Materials and Manufacture*, vol. 6, no. 4, pp. 494–507, Dec. 2023, doi: 10.1016/j.ijlmm.2023.05.002.

ANNEX I

Table A.1 — Flexural (Onyx®), 0°/90° build orientation

F-O-NF-0.90			
Specimen	**Weight (g)**	**b (mm)**	**h (mm)**
1	3.68	10.15	4.12
2	3.67	10.16	4.11
3	3.68	10.13	4.15
4	3.66	10.14	4.08
5*	4.00	10.27	4.11
Average	**3.67**	**10.15**	**4.12**
Standard deviation	**0.01**	**0.01**	**0.03**

Notes:
b = average of three width measurements (b1, b2, b3); h = average of three thickness measurements (h1, h2, h3).
* Specimen recorded in the source data as manufactured incorrectly; kept in the table but excluded from the Average and Standard deviation.

Table A.2 — Flexural (Onyx®), 45°/-45° build orientation

F-O-NF-45.45			
Specimen	**Weight (g)**	**b (mm)**	**h (mm)**
1	3.53	9.89	4.07
2	3.53	9.96	4.08
3	3.58	9.99	4.03
4	3.53	9.99	4.10
Average	**3.54**	**9.96**	**4.07**
Standard deviation	**0.03**	**0.05**	**0.03**

Notes:
b = average of three width measurements (b1, b2, b3); h = average of three thickness measurements (h1, h2, h3). No specimens excluded.

Table A.3 — Flexural (Continuous Carbon Fibre), 0°/90° build orientation

F-F-0-0.90			
Specimen	**Weight (g)**	**b (mm)**	**h (mm)**
1†	—	15.00	2.00
2†	—	15.00	2.00
3†	—	15.00	2.00
4†	—	15.00	2.00
5†	—	15.00	2.00
Average	**—**	**15.00**	**2.00**
Standard deviation	**—**	**0.00**	**0.00**

Notes:
b = average of three width measurements (b1, b2, b3); h = average of three thickness measurements (h1, h2, h3).
† Original width, thickness and weight measurements for this series were lost. Nominal values (b = 15.00 mm, h = 2.00 mm) were assumed for all specimens instead of measured values. Standard deviation is therefore 0.00 by construction, not a measured spread.

Table A.4 — Flexural (Continuous Carbon Fibre), 45°/-45° build orientation

F-F-0-45.45			
Specimen	**Weight (g)**	**b (mm)**	**h (mm)**
1†	—	15.00	2.00
2†	—	15.00	2.00
3†	—	15.00	2.00
4†	—	15.00	2.00
5†	—	15.00	2.00
Average	**—**	**15.00**	**2.00**
Standard deviation	**—**	**0.00**	**0.00**

Notes:
b = average of three width measurements (b1, b2, b3); h = average of three thickness measurements (h1, h2, h3). † Original width, thickness and weight measurements for this series were lost. Nominal values (b = 15.00 mm, h = 2.00 mm) were assumed for all specimens instead of measured values.

Table A.5 — Tensile (Onyx®), 0°/90° build orientation

T-O-NF-0.90			
Specimen	**Weight (g)**	**b (mm)**	**h (mm)**
1	9.34	10.14	4.06
2	9.43	10.22	4.07
3	9.42	10.16	4.07
4	9.44	10.19	4.15
5	9.44	10.20	4.15
Average	**9.41**	**10.18**	**4.09**
Standard deviation	**0.05**	**0.03**	**0.04**

Notes:
b = average of three width measurements (b1.1, b1.2, b1.3); h = average of three thickness measurements (h1, h2, h3).

Table A.6 — Tensile (Onyx®), 45°/-45° build orientation

T-O-NF-45.45			
Specimen	**Weight (g)**	**b (mm)**	**h (mm)**
1	9.25	10.01	4.12
2	9.35	10.04	4.14
3	9.31	10.03	4.12
4	9.35	10.02	4.14
5†	—	10.25	4.15
Average	**9.32**	**10.07**	**4.13**
Standard deviation	**0.05**	**0.10**	**0.01**

Notes:
b = average of three width measurements (b1.1, b1.2, b1.3); h = average of three thickness measurements (h1, h2, h3).
† Specimen 5 weight not recorded in the source data.

Table A.7 — Tensile (Continuous Carbon Fibre 0°/90°), 0°/90° build orientation

T-F-0-0.90			
Specimen	**Weight (g)**	**b (mm)**	**h (mm)**
1	14.82	25.06	2.21
2	14.98	25.00	2.14
3	14.90	25.00	2.22
4	14.91	25.00	2.08
5	14.81	25.03	2.15
6	11.99	25.01	2.15
7	12.15	24.99	2.06
8	11.30	24.86	2.14
Average	**13.73**	**24.99**	**2.14**
Standard deviation	**1.61**	**0.06**	**0.06**

Notes:
b = average of three width measurements (b1.1, b1.2, b1.3); h = average of three thickness measurements (h1, h2, h3).

Table A.8 — Flexural Sandwich, 0°/90° build orientation

S-F-0-0.90			
Specimen	**Weight (g)**	**b (mm)**	**h (mm)**
1	53.30	39.43	8.24
2	53.16	39.17	8.16
3	53.90	39.04	8.05
Average	**53.45**	**39.21**	**8.15**
Standard deviation	**0.39**	**0.20**	**0.10**

Notes:
b = average of three width measurements (b1, b2, b3); h = average of three thickness measurements (h1, h2, h3).